Determining relative age of out-of-sequence faults: integration of foreland basin deposits to a flexural thrust belt evolution and a case study in Western Nepal

by

Joshua E. S. Olsen

BS, Wheaton College, 2014

Submitted to the Graduate Faculty of

the Dietrich School of Arts and Sciences in partial fulfillment

of the requirements for the degree of

Master of Science

University of Pittsburgh

2017

UNIVERSITY OF PITTSBURGH

Dietrich School of Arts and Sciences

This thesis was presented

by

Joshua E. S. Olsen

It was defended on

September, 28, 2017

and approved by

Charles E. Jones, Ph D
Senior Lecturer,
Geology and Environmental Science
Dietrich School of Arts and Sciences
University of Pittsburgh

Eitan Shelef, Ph D
Assistant Professor,
Geology and Environmental Science
Dietrich School of Arts and Sciences
University of Pittsburgh

Thesis Director: Nadine McQuarrie, Ph D
Associate Professor,
Geology and Environmental Science
Dietrich School of Arts and Sciences
University of Pittsburgh

DETERMINING RELATIVE AGE OF OUT-OF-SEQUENCE FAULTS: INTEGRATION OF FORELAND BASIN DEPOSITS TO A FLEXURAL THRUST BELT EVOLUTION AND A CASE STUDY IN WESTERN NEPAL

Joshua E. S. Olsen, M.S.

University of Pittsburgh, 2017

Forward modeled, balanced cross sections, accounting for both flexural loading and erosional unloading have the potential to verify and refine the kinematic sequence of deformation in fold and thrust belts. Insight into the relative order of events is particularly apparent for out-of-sequence faults that have the ability to either vertically exhume deeper strata in the case of thrusts, or normal faults which create basins that may or may not be preserved in the mapped geology. Strata exhumed by thrusts (either in- or out-of-sequence) may leave a distinct provenance or detrital age signature in the foreland basin. The foreland basin evolution can be predicted with the isostatic modeling, allowing correlation between modeled and measured stratigraphic sections near the cross section. Incremental modeling in short displacement steps creates "pseudostratigraphy" in the foreland which predicts the location and magnitude of preserved sediment, and identifies the location and amount of material eroded in the incremental thrust event, i.e. the provenance of the sediments within the pseudostratigraphy. We present a case study for this method using two cross sections through the Himalayas of Far-Western Nepal (Api and Simikot) and assess the validity of the resulting dated kinematic histories, displacement rates, flexural wave response, section geometry, and matches to provenance for both sections. We also compare flexural forward models with and without an additional sediment loading modeling step, and find that while sediment loading does not have a large effect on the kinematic orders inferred from flexural modeling, it does affect precision in

correlating model steps to paleomagnetic ages (±1 Ma). In order to reproduce the foreland provenance we argue that OOS thrust and normal faults in the Api section occurred between 11-4 Ma. In addition, we propose that shortening estimates for the Simikot cross section are too high (> 50 km) which causes unrealistic deformation rates up to 80 mm/yr between 25-20 Ma. We conclude that the flexural forward modeling method has a vast potential for revising the kinematics of fold-and-thrust belt cross sections when the full foreland basin evolution is considered.

TABLE OF CONTENTS

LIST OF TABLES

LIST OF FIGURES

1.0 INTRODUCTION

Fold-and-thrust belts are characterized by the generally foreland-ward propagation of thrust faults, a distinguishing feature first identified by Armstrong and Oriel (1965), and Bally et al. (1966). Deeper in the orogen, thrust bound slices of rocks (horses) tend to stack into duplex structures that strongly suggest (and sometimes require) a systematic foreland propagation of thrust structures (Boyer and Elliott, 1982; Butler, 1987). Balanced cross sections (e.g. Dahlstrom, 1969) constructed through mountain belts propose a relative thrusting order necessary to recreate the cross section geometry, but there is a strong potential for multiple, valid balanced cross section geometries that all match the same surficial observations. While a relative sequence of structural development may be possible to determine, either from the geometry of a duplex (Boyer and Elliott, 1982) or the successive rotation of preceding faults in an imbricate fan (Suppe, 1980; Shaw et al., 1999), constraining the age of fault motion is more challenging. Faults near the foreland, which are often the most recently active, may be dated by the youngest age of synorogenic rocks that they cross cut and the dating of associated conglomerate deposits in the foreland (e.g. Jordan, 1981; Jordan et al., 1988; Bullen et al., 2001; Echavarria et al., 2003). Additionally, currently active faulting in the foreland or hinterland may be recognized by strong geomorphic signals such as steepened river profiles and remnant topographies (Lave and Avouac, 1999; Wobus et al., 2003; Kirby and Whipple, 2012). However, while these methods are easy to employ for young and active faults, older faults will always have little stratigraphic or geomorphic indicators preserved and potentially were far removed (in time and space) from the modern foreland when these faults were active. On rare occasions, older thrust faults can be

dated on the basis of cross cutting relationships, as was used to first interpret foreland-propagation of thrusts (Armstrong and Oriel, 1965; Bally et al., 1966) but these dates are often very imprecise and may be speculative. Where the thrust zone is well preserved and has reached the appropriate thermal conditions, a more accurate date may be acquired by dating of illite gouge produced in shallow crustal faults (Vrolijk and Van Der Pluijm, 1999), a method which has been useful for dating fault activity on a timescale of tens of millions of years, (van der Pluijm et al., 2001; Duvall et al., 2011; Rahl et al., 2011), and may also illuminate out-of-sequence (OOS) thrusting in the hinterland (van der Pluijm et al., 2006; Rahl et al., 2011).

OOS faults are faults which occur in collisional fold-and-thrust belts outside of a regular order of fault propagation towards the foreland (Morley, 1988). They are a fundamental aspect of deformation in fold-and-thrust belts, and have been observed and interpreted frequently throughout the Himalayas (Schelling, 1992; Srivastava and Mitra, 1994; DeCelles et al., 2001; Wobus et al., 2003; Robinson et al., 2006; Long et al., 2012; Mukherjee, 2015). They are also proposed for the Zagros Mountains (Molinaro et al., 2005), the Pyrenees (Rahl et al., 2011), the Alps (Castellarin and Cantelli, 2000), the Canadian Cordillera (van der Pluijm et al., 2006) and the Andes (Rak et al., 2017). Typically, these faults run along the planes of previous thrust faults in a reactivation of deformation, an effect which can be accentuated by erosion and breaching of the overriding roof thrust and thus removal of load above older fault planes (Cruz et al., 2010; Malavieille, 2010)., In some cases OOS faults may also cut through strata of other thrust sheets and cause unexpected repetition of stratigraphy at the surface (e.g. Robinson et al., 2006; Robinson and Martin, 2014; DeCelles et al., 2001). OOS reverse-fault motion along the original path of an earlier in-sequence fault makes these OOS faults difficult to discern during regular field mapping and cross section interpretation (Morley, 1988; Cruz et al., 2010). OOS normal

and thrust faults (referred to together from here on as "*OOS faults*") have the potential to occur in any orogenic wedge (Dahlen et al., 1984; Graveleau et al., 2012). Critical wedge theory (Dahlen et al., 1984) argues that OOS faults occur as a specific response to changes in the critical state of an orogenic wedge. Large jumps in foreland propagation or focused erosion in the hinterland cause the topographic angle (α) to be lowered below the critical taper angle (Dahlen, 1990). In order to maintain a critical state – where every point in the actively deforming material is at the verge of failure and deforming self-similarly, a fold-thrust belt at a sub-critical taper may deform internally through the creation or activation of duplexes *or* by activation of OOS thrusts in the hinterland to raise the topographic angle. Indeed, OOS thrusts may actually be the preferred method for achieving this end due to their strongly vertical component of motion which causes fast thickening of the wedge with minimal work, particularly if a duplex already exists in the hinterland allowing for prior thrust planes to be reactivated (Graveleau et al., 2012). Similarly, it logically follows that super-critical tapers are forced to reduce their topographic angle through increased erosion, forelandward propagation, *or* OOS normal faults. Thus, OOS faults represent the natural response of a thrust belt structure to changing wedge conditions (Morley, 1988).

Traditionally, when restoring balanced cross sections with OOS faults of unknown age researchers have had no choice but to place them at the chronological end of their kinematic sequences (e.g. Robinson, 2008). The reason for this simplification is that no purely geometric constraints govern the age of OOS faults, apart from simple cross-cutting relationships of strata and thrust sheets. Thus, it is geometrically valid to say that these faults occur after primary deformation in the orogeny. However, if a cross section is sequentially restored while taking into account isostatic thrust loading, estimates of paleotopography and the resulting erosion and

sedimentary fill, a suite of previously unrecognized constraints and proxies for the timing of these faults emerge. Examples of these include the preservation of normal fault basins or timing of provenance indicators recorded in the foreland basin, which is particularly sensitive to changes in erosion induced exhumation including increased vertical exhumation caused by OOS thrusts. Additionally, geomorphological signals of recent, active uplift (e.g. Wobus et al., 2003; Harvey et al., 2015; Mugnier et al., 1994) can be used to identify location and age of motion on a recently active OOS fault. The order in which OOS faults occur has a significant effect on the geology preserved at the surface, highlighting the opportunity for flexural and isostatic modeling to produce better constrained and thus more realistic kinematic reconstructions.

This paper will evaluate the use of isostatic forward modeling of fold-and-thrust belt cross sections (McQuarrie and Ehlers, 2015, 2017) to evaluate viable relative timing of OOS faults in the far western Himalaya by using the requirement that the isostatically balanced forward model must both recreate the known geology at the surface today and reproduce the provenance of the foreland basin stratigraphy. Isostatically balanced forward modeling takes into account the flexure of the lithosphere, erosion, and deposition of foreland sedimentary fill occurring at each step. Thus, foreland basin sediments may record changes in structural configuration if the change produces a distinct provenance record such as a pronounced change in detrital zircon ages or εNd signatures. Specifically, in this paper we will use The Api and Simikot cross sections from the Western Nepal Himalayas originally interpreted by Robinson et al. (2006) (Fig. 1, A-A' and B-B', respectively). In both these sections, OOS faults were proposed as necessary structures needed to match the surface geology, but chronologically they were placed at the very end of the sequential reconstructions (Robinson, 2008). We argue that

the process of kinematic and isostatic modeling can constrain the kinematic order of these faults and the resulting topographic signature.

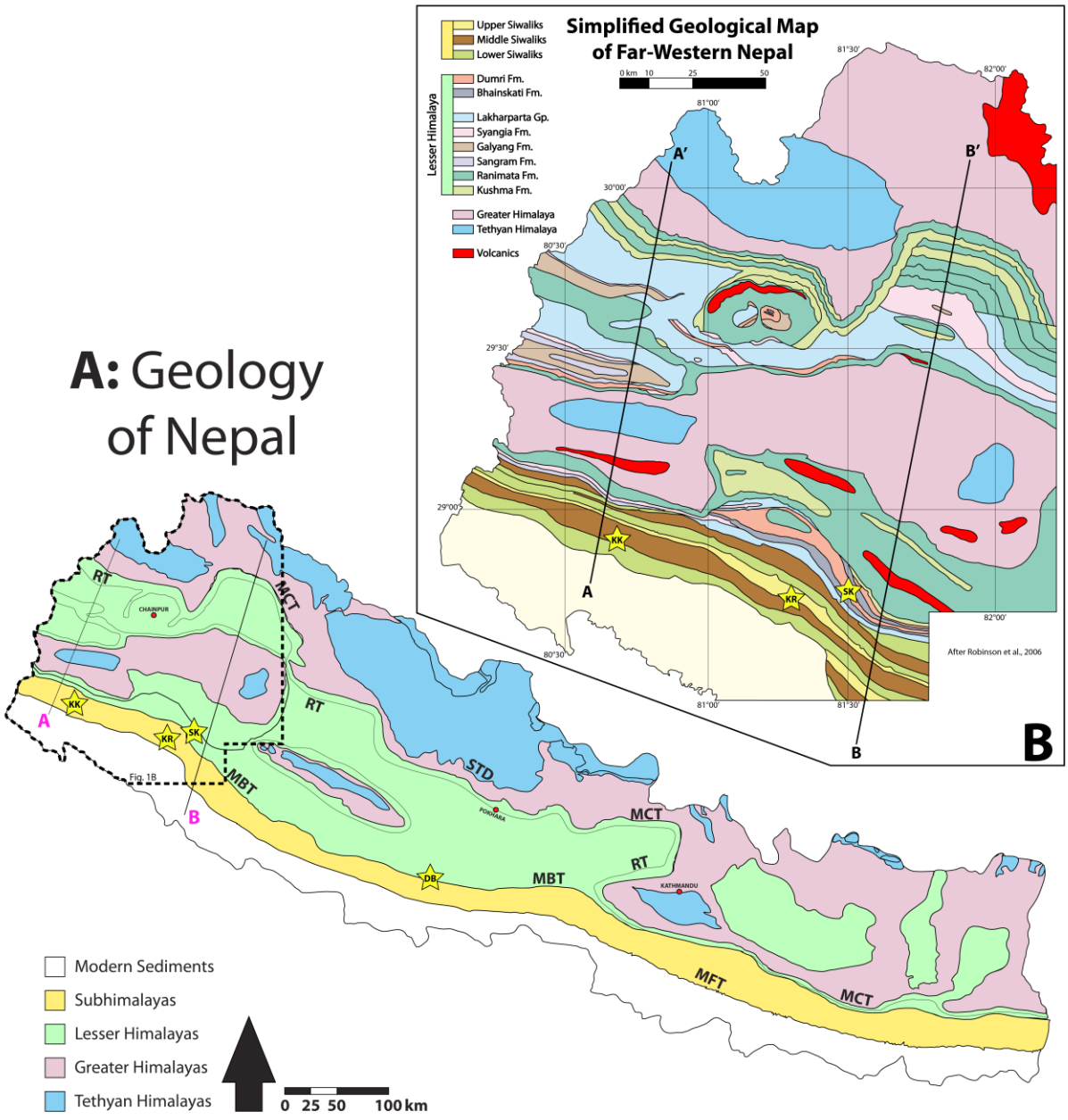

Figure 1. (A) Geology of the Himalayas in Nepal with cross section traces of Api (A) and Simikot (B). KK = Khutia Khola, KR = Karnali River, SK = Swat Khola, DB = Dumri Bridge, (B) Simplified map of the Geology of Far Western Nepal after Robinson et al., (2006)

2.0 GEOLOGIC BACKGROUND

Western Nepal is divided into four major tectonostratigraphic zones (Fig. 1) which are segregated by major thrusts faults and/or shear zones (Gansser, 1964). From hinterland to foreland (north to south) these are the South Tibetan Detachment, Main Central Thrust (MCT), Ramgarh Thrust (RT), Main Boundary Thrust and the Main Frontal Thrust (MFT). The South Tibetan Detachment is a top-to-the-north shear zone which was active in the early Miocene but also displays Miocene to modern normal fault activity (Burchfiel et al., 1992; Coleman, 1996; Hodges et al., 2001). The South Tibetan Detachment places the Cambrian to Eocene low-grade metasedimentary to sedimentary strata of the Tibetan/Tethyan Himalayas over the high grade metamorphic rocks (amphibolite-grade schist, orthogneiss and paragneiss) of the Greater Himalayas (GH). GH rocks are bound in the south by the MCT which places GH rocks over ~160-220 km of phyllitic and quartzite rich rocks of the lower Lesser Himalayas (LH). This thrusting initiated at ~25 Ma on the basis of $^{40}Ar/^{39}Ar$ muscovite cooling age from the GH in far western Nepal (Robinson et al., 2006) The lower LH rocks immediately under the MCT are displaced by the RT, which forms the roof thrust of the underlying Lesser Himalayan Duplex (LHD). The LHD consists of stacked thrust slices (horses) of lower LH rocks and upper LH quartzite, phyllite, and carbonate rocks. The LHD is partly covered by a klippe (in Western Nepal, the Dadeldhura Klippe, DK) of the RT and MCT sheets. The LHD's southern limit is the Main Boundary Thrust. South of the Main Boundary Thrust, the MFT and various other thrusts

of the Sub-Himalayan Thrust System repeat the units of the Tertiary age Sub-Himalayas (SH) or Siwalik Group foreland basin deposits (DeCelles et al., 1998; DeCelles et al., 2001; Robinson et al., 2006).

2.1 FORELAND STRATIGRAPHY

The Earliest foreland basin strata include the Bhainskati Formation (54-41 Ma) and the Dumri Formation (21-16 Ma) (DeCelles, Gehrels, Quade, and Ojha, 1998). The overlying Siwalik Group preserves foreland basin sediments that were deposited between ~15 and 1 Ma (Mugnier et al., 1999; Ojha et al., 2000; DeCelles et al., 1998).

The Bhainskati Formation in Far Western Nepal (along the Simikot section) is a 100-200 m thick unit of sandstone and organically modified shale/mudstone (Sakai, 1983; Robinson et al., 2006) topped by an unconformity and well-developed oxisol. However, this unit is only observed along the trace of the Simikot section, and not the Api section. The Bhainskati sediments are interpreted to have accumulated in a shallow back-bulge depozone between the Indian craton and the forebulge while the oxisol is interpreted to represent subaerial exposure due to the passage of the forebulge (DeCelles and Giles, 1996; DeCelles, Gehrels, Quade, and Ojha, 1998).

Unconformably overlying the Bhainskati Formation, the Dumri is composed of gray-green sandstone interbedded with red mudstones, and is typically ~1300 m thick (DeCelles et al., 1998). In the Api section the thickness of this formation is measured only at 250 m, and at Simikot it is up to ~700 m thick (Robinson et al., 2006). In Western Nepal along the Seti River (north of the Karnali River, KR star in Fig. 1), the Dumri formation was deposited from 20-16 Ma (DeCelles et al., 2001; Ojha et al., 2009).

The contact between the Dumri and the overlying Siwalik Group rocks has never been observed in the field and is thus poorly defined. The three Siwalik Group divisions (Lower, Middle, and Upper) are based on lithostratigraphic changes rather than chronostratigraphic transitions. The Lower Siwalik member consists of interbedded fluvial sandstones and mudstones and in the area of Khutia Kohla (KK star near A-A', Fig. 1) it is approximately 1500 m) to 2000 m thick at Simikot (Robinson et al., 2006). The Middle member is thicker, on the order of 3000 m (at Api) and 2500 m (at Simikot), and is a coarsening upward sequence of fluvial mud and sandstones at base with increasing number and thickness of sandstone and conglomerate beds towards the top (DeCelles, Gehrels, Quade, and Ojha, 1998; Robinson et al., 2006). At Khutia Khola, the Lower-Middle contact has been dated at 10.8 Ma, and there is no exposure of the top of the Middle unit (Ojha et al., 2000). While the Middle-Upper contact is not exposed in Western Nepal, where it is exposed in eastern Nepal it has been dated to 4.5 Ma (DeCelles et al., 1998). The Upper Siwalik unit is mostly conglomerates deposited in a proximal foreland environment. The exposed sections in western Nepal range between 1000 m (Api) to 2500 m (Simikot) but is repeatedly truncated by Sub-Himalayan Thrust System faults. The top of this unit was deposited between 1 and 2 Ma on the basis of bio- and magnetostratigraphy (Mugnier et al., 1999); it is currently being actively buried by modern alluvium.

2.2 PROVENANCE OF FORELAND BASIN DEPOSITS

The εNd of the foreland basin strata from the Bhainskati to the Upper Siwaliks at Khutia Khola and other sample locations is detailed in Fig. 2. Robinson et al. (2001) showed that the LH exhibit significantly more negative εNd values than either the Tethyan Himalayas or GH due

to its older age and that the εNd signal in the foreland basin stratigraphy will become more negative when the LHD is breached and the LH starts eroding, producing an influx of strongly negative εNd detritus in the foreland. In the ~4.5 km thick measured section of Siwaliks at Kutia Khola, measured εNd values become notably more negative between 0.9-1.5 km above the lowest sampled Lower Siwalik material (values shown by red curve in Fig. 2a, location shown in Fig. 1). The measured stratigraphic section does not account for the full thickness of the Lower Siwalik unit since the base has not been observed. Based on mapped contacts, the Lower Siwalik unit in the Api region is approximately 0.8 km thicker than at Simikot (Robinson et al., 2006), suggesting the LH detritus signal should be present 1.7-2.3 km above the MFT. The minimum thickness for this signal (1.7 km above the MFT) is approximately equal to 10-11 Ma based magnetic stratigraphy at Khutia Khola (Ojha et al., 2000). However, because of the εNd sample spacing in Robinson et al., (2001) we argue that the actual stratigraphic level of LH detritus could be as high as 2.3 km above the MFT (see Fig. 2a). Additionally, the sharp decrease in εNd from the Bhainskati to the Dumri Fms. is interpreted to indicate the first erosion of the GH units (Robinson et al., 2001).

Other provenance and detrital zircon age studies substantiate these claims but also show a change in provenance from east to west. In the east, the Dumri Formation observed at Dumri Bridge exhibits an increase in plagioclase content over the Bhainskati and contains detritus derived from sedimentary and metasedimentary units interpreted to be GH and Tethyan Himalayas. In addition, the Dumri has U-Pb detrital zircon age populations that mirror those of GH and Tethyan Himalayas rocks (DeCelles et al., 1998). In the west at Khutia Khola, provenance of foreland deposits through the Lower and Middle Siwaliks show a marked increase in K-feldspar rich metasediment, interpreted as being derived from GH rocks metamorphosed in

the DT (DeCelles, Gehrels, Quade, Ojha, et al., 1998) with the upper portion of the Lower Siwaliks containing the first appearance of kyanite and sillimanite clasts, clearly indicative of GH provenance. These minerals imply that in far western Nepal (and thus the Api section), GH erosion, through a significant portion of the MCT, occurred later at Api than at Dumri Bridge (DeCelles, Gehrels, Quade, Ojha, et al., 1998). Additionally, metacarbonate clasts in the middle Siwaliks at Khutia Khola, characteristic of LH material, accompany an increase in detrital zircon age and $^{87}Sr/^{86}Sr$ values (DeCelles et al., 1998). This east west spatial variability – where the Api and Simikot sections are ~100 km apart – is important and implies a different erosional and depositional history between central and western Nepal, that should be reflected in the modeling.

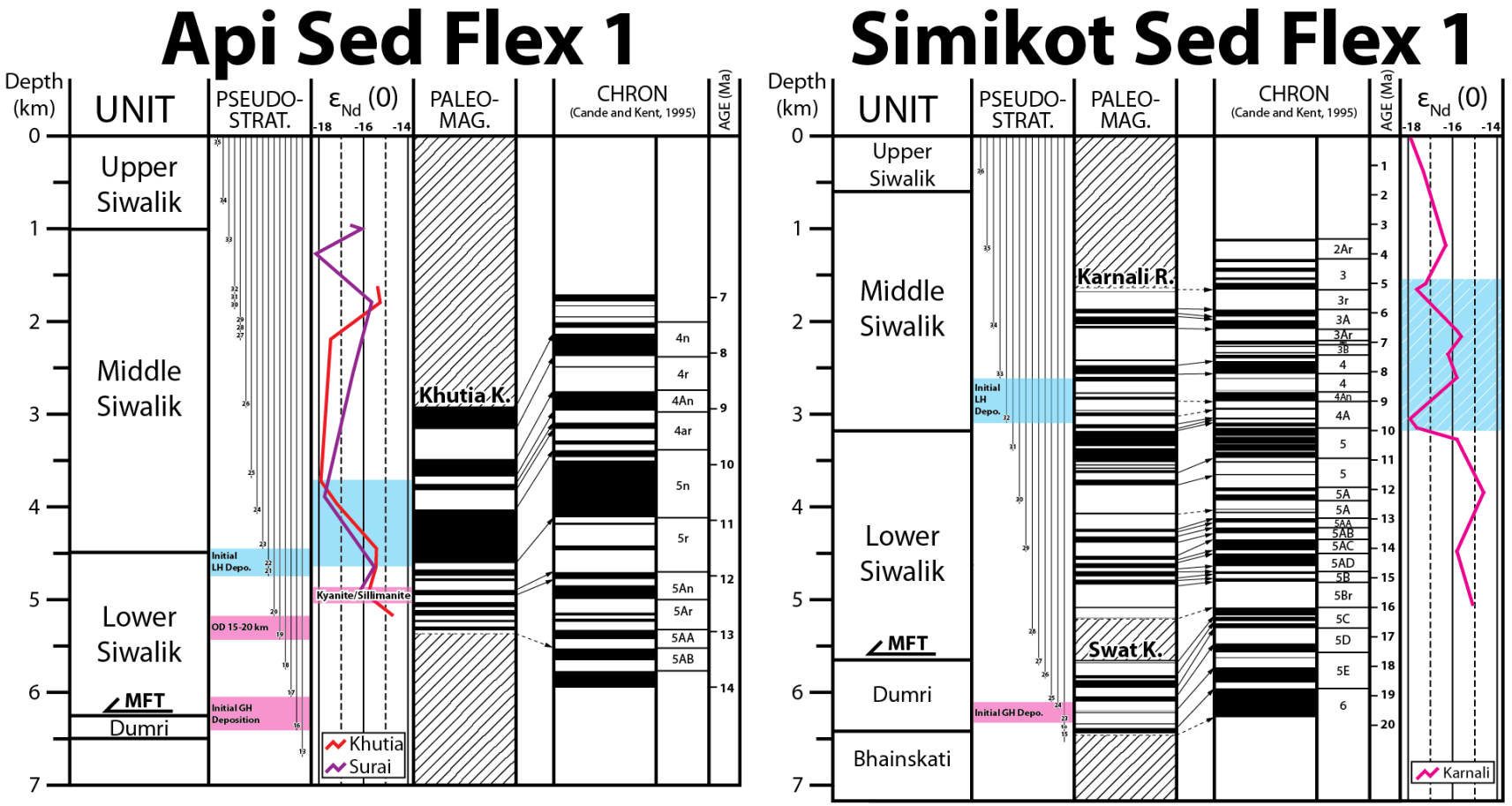

Figure 2. Stratigraphy, paleomagnetic correlations, and εNd values of the foreland basin sediments as measured from the cutoff of the MFT in the Api (A) and Simikot (B) sections. Depths/thickness measured bedding-parallel. Api paleomagnetic stratigraphy comes from (Ojha et al., 2000), Simikot from both (Guatam and Fujiwara, 2000; Ojha et al., 2009) both utilizing the geomagnetic polarity timescale of (Cande and Kent, 1995). εNd curves after (Robinson et al., 2001) and (Szulc et al., 2006) for Api and Simikot, respectively. Modeled pseudo-stratigraphy depths measured in the same fashion as stratigraphic depth/thicknesses. OD = Original Depth of GH material eroded and deposited at this stage was between 15-20 km, the general depth of Kyanite Formation.

2.3 BALANCED CROSS SECTIONS THROUGH WESTERN NEPAL

Balanced cross sections provide a geometrically valid and permissible interpretation of the subsurface through fold and thrust belts (Dahlstrom, 1969). The two cross sections that will be utilized in this paper for flexural and erosional modeling are the Api and Simikot sections from far western Nepal (after Robinson et al., 2006) (sections A and B, respectively in Fig. 1). The Api section in particular (Robinson, 2006) offers the best case study for determining the order of faulting with four normal faults and two OOS thrusts whose sequence is unknown. The Simikot section used in this study is a modified version of the Robinson et al. (2006) original cross section. Recent observations of high river steepness indices and seismic patterns suggest two regions of active uplift in far western Nepal (Harvey et al., 2015). These regions, termed physiographic transition north (PT2-N) and south (PT2-S) (Harvey et al., 2015) were co-located with active footwall ramps in the revised cross section and in the case of PT2-N, co-located with the OOS thrust mapped by Robinson et al. (2006).

3.0 METHODS

Flexural and erosional modeling of the Api and Simikot sections was performed using Midland Valley's 2D Move software following the process of McQuarrie and Ehlers (2015). In the first phase of modeling, a sequential kinematic model (e.g. Robinson, 2008) was created from the systematic faulting of the undeformed cross section to reproduce the published cross section geometry. The entire modeling process is summarized in Fig. 3 and explained in detail below.

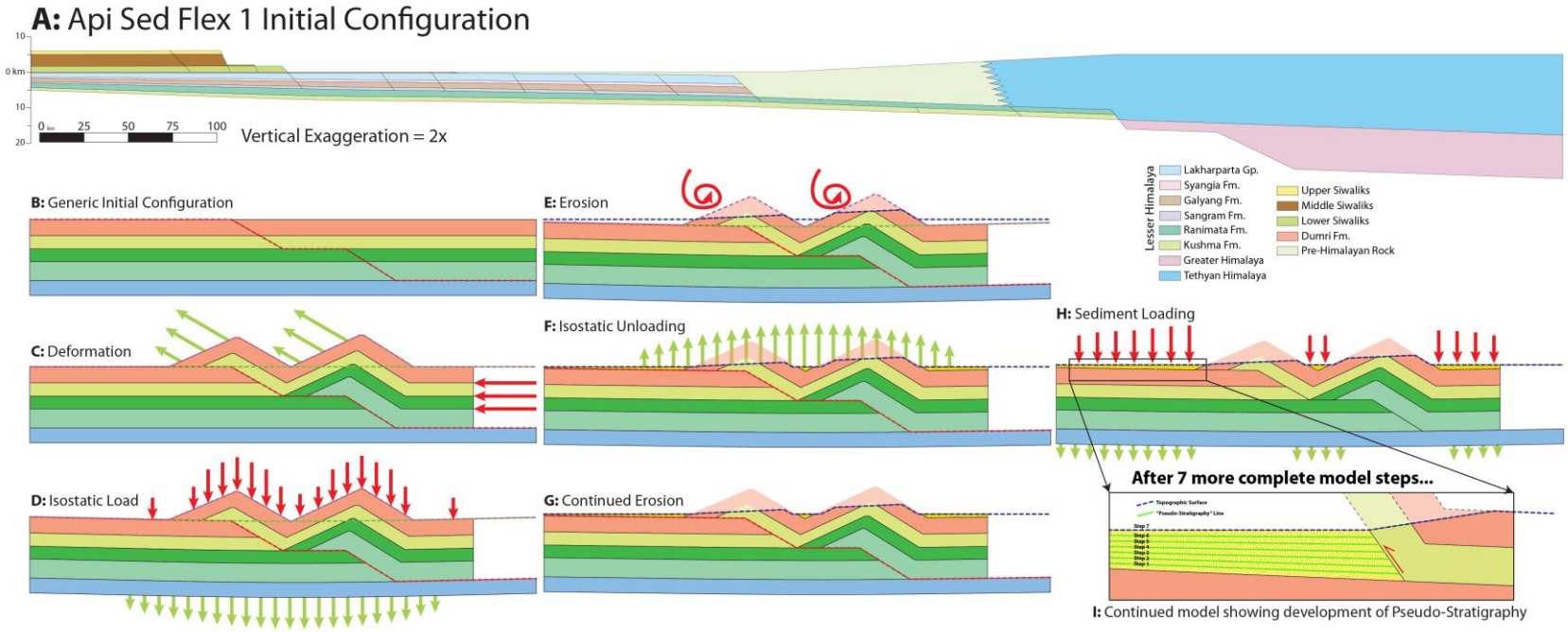

Figure 3. (A) Initial configuration of the Api Sed Flex 1 model, shown as an example of the initial conditions of the MOVE models, (B-H) Cartoons illustrating the general flexural and erosional modeling method with additional sediment loading step, (I) Closeup of the foreland after continued modeling which produces a package of "Pseudo-Stratigraphy" which can be correlated to other stratigraphic studies.

3.1 INITIAL MODEL CONFIGURATION

The isostatic model begins with an initial horizontal-to-gently-dipping stratigraphic basin geometry (initial taper) of the LH strata before activation of the MCT at ~25 Ma (Fig. 3a). This times slice represents the Himalyas after the formation of the Tethyan fold-thrust belt (Ratschbacher et al., 1994; Murphy and Yin, 2003; McQuarrie and Ehlers, 2015), but before deformation on the MCT (DeCelles et al., 2001; Robinson et al., 2006; Robinson and McQuarrie, 2012). In our original configuration, we show a gently north-dipping (0.5-1°) Indian margin, where Cretaceous rocks are at approximate sea level from the modern foreland to the northern extent of modeled Tethyan rocks. In addition, the elevation of the LH stratigraphy (and thus the entire section) in the successful models was lowered such that the top of the Lakharpata group at the lower cutoff of the MFT was at a depth of -0.29 km (for Api) and -1.84 km (for Simikot) depth to prevent erosion of the pre-himalayan Lakharpata group or Bhainskati Formation due to the migrating forebulge, requiring that the Bhainskati formation was initially about 1 km thicker at Simikot and was most likely present along the Api section before forebulge erosion. Additionally, we assume that this ancient Tethyan Himalayan belt had a similar topographic taper angle (□□ to the modern Himalayas (~1.5-2°) and that the height of that orogen reached an elevation of 5 km (DeCelles et al., 2007; Hetzel et al., 2011; Rohrmann et al., 2012). This assumption allows the Greater Himalayas to be buried to a depth of ~30 km, to match peak pressure and temperature conditions recorded in these rocks (Kohn, 2008).

3.2 ISOSTATIC MODELING

Displacements along faults were modeled in 20 km increments. Each increment of deformation created an uplifted topographic surface above ramps in the decollement and at the deformation front (Fig. 3c). This uplift produces an elevation difference between the pre-deformation topography and the newly deformed topography. The vertical 2D area between these surfaces gives the size and distribution of the isostatic load (McQuarrie and Ehlers, 2015; Rak, 2017 (in review)), which flexurally depresses the lithosphere (Fig. 3d). The wavelength over which the load is compensated is determined by the flexural properties of the lithosphere, calculated assuming a series of ~1 km wide rectangular loads on an infinite plate (Turcotte and Schubert, 1982). In 2D Move, lithospheric flexure variables include the bulk density of the load and the effective elastic thickness (EET) of the lithosphere (Table 1). The loaded, deformed topography is used to create a new topography by simulating the magnitude of erosion needed to create a topographic taper angle (α), based on the current average relief across the western Nepal Himalayas. This topographic angle normally ranges from 1.5-2.0° in western and central Nepal, but locally can reach angles of 4° over distances of 50-70 km (Harvey et al., 2015). Modeled α varied between 1.6-2.5º, and were based on both the modeled location of the deformation front (longer distances are reflected in lower α values) and erosion requirements to match foreland basin observations. These values are well within the average lower limits for fold-and-thrust belts and accretionary wedges (~1.0-4.5°, Lallemand et al., 1994) and match modern values (1-4°) calculated across the Himalaya from Nepal to Bhutan (Duncan et al., 2003).

All strata projected above the newly created topography are instantaneously removed via erosion and the section isostatically rebounds (Fig. 3e, f). The areas in the foreland that subside below sea level (due to the flexural distribution of the thrust load) are assumed to collect

sediment and are filled to 0 km in elevation. The eroded stratigraphy above the newly created topography is the provenance source for each increment of the model and subsequent foreland basin fill. Throughout the modeling process, the 0 elevation lines in the foreland are preserved, creating a package of "pseudo-stratigraphy" (Fig. 3i) with a definite provenance.

The isostatic modeling was performed both ignoring the isostatic load of the sedimentary basin and accounting for the sediment load by assigning a density (2200-2300 kg/km^3, see Table 1) to the pseudo-stratigraphic increment created at each step (Fig. 3h). Without this additional sediment loading step, the bulk rock density used to create the final best-fit sections ranged between 2750-2850 kg/km^3, and with sediment loading, the ideal bulk rock density was 2500-2550 kg/km^3 (Table 1). The additional sediment load redistributes the isostatic response, changes the flexural wavelength, and requires a lower bulk rock density to achieve the same fit.

Multiple kinematic and flexural models were run systematically varying density, EET, α, and the kinematic sequence of deformation until the following key characteristics matched the measured field data; (1) surface geology including exposed units, dips, and the appropriate absence or preservation of any normal fault basins, (2) decollement angle and topography (β and α, respectively, e.g. Dahlen et al., 1983), and (3) foreland signals of provenance, i.e. a match between the modeled pseudo-stratigraphy and measured foreland stratigraphic sections (e.g. Robinson et al., 2001; DeCelles, Gehrels, Quade, and Ojha, 1998; DeCelles, Gehrels, Quade, Ojha, et al., 1998; DeCelles et al., 2001; Ojha et al., 2000, 2009). If the final step did not match these proxies, it was run again with different parameters until a best-fit solution was systematically achieved.

Cross Section Name	Model Name	Total Displacement (km)	Bulk Rock Density (kg/m^3)	Sediment Density (kg/m^3)	Initial Restoration Depth (km*)	EET (km)	Erosion Angle/s (°)	Final Decollement Angle (°)	GH Erosion occurs at… (km displacement)	GH Deposition Depth (km**)	LH Erosion occurs at… (km displacement)	LH Deposition Depth (km**)	Good final model match?	Notes	Paper Section(s)	Figure(s)
Api	Api Flex 1	561.4	2800	**N/A**	0	65	2-2.5	5.12-6.26	494.4	~5.9 (in Mid. Siwalik Mbr., very late)	549.6	Not preserved in MFT sheet (too late)	NO	Normal faults at chronological end, causes ~10.5 km deep basin. Hinterland 7 km too deep, decollement angle too steep (6.3 vs ~4deg). Overall final geometry does not match well, initial restored section needed revision.	4.1.1.	4
Api	Api Flex 2	548.02	2650	**N/A**	-0.75	80	1.5-2	4.29-4.79	369.4	0.951 (late)	481.39	4.2 (very late)	NO	Decollement depth and angle good, slightly shallow in foreland, surface geology good, normal fault basin only about 1 km deep, BUT erosion and deposition too late.	4.1.2.	4
Api	Api Flex 3	548.02	2750	**N/A**	-0.29	90	1.65 -2.0	4.18-4.26	331.35	-0.174	415.85	1.429	YES	~ 1 km too shallow in both foreland and hinterland, but good match with surface and erosion/deposition, normal fault basin present but only 0.95 km deep by 4.19 km wide.	4.1.3.	4
Api	Api Sed Flex 1	548.02	2500	2200	-0.29	70	1.65 - 2.15	4.55-3.94	331.35	0.2	415.85	1.787	YES	Accounting for sediment loading produced the best Api match. Normal fault basin present but only 0.78 km deep by 3.51 km wide. Surficial geology and provenance match well.	4.1.4. 4.1.5.	3, 4, 5
Simikot	Simikot Flex 1	872.45	2850	**N/A**	-1.84	100	1.6	4.5-5.2	580.36	-1.12	719.27	2.865	NO	Decollement angle is ~2° too steep, which results in a foreland that is 2 km too shallow. EET is the highest allowable value. Provenance is within reason. Best possible non-sediment load match within limitations.	4.2.1.	7
Simikot	Simikot Sed Flex 1	872.45	2550	2300	-1.84	95	1.6	4.04-4.26	503.1	-1.05	722.14	4.038	YES	Sediment loading method produced the closest and most realistic result. Depositional depths, and surface geology match closely, with a decollement that is only about 0.5 km too shallow in the foreland and 0.8 km too deep in the hinterland.	4.2.2. 4.2.3.	7

* Elevation of Lakharparta below the lower cutoff point of the MFT, ** bedding-perpendicular distance +above/-below the lower cutoff point of the MFT (Above = within Siwalik group, Below = within Dumri Fm.)

Table 1. Flexural Model Parameters and Final Results

	Api Flex 1		Api Flex 2		Api Flex 3		Api Sed Flex 1		Simikot Flex 1		Simikot Sed Flex 1	
	Fault Name	Disp. (km)	Fault Name	Disp. (km)	Fault Name	Disp. (km)	Fault Name	Disp. (km)	Fault Name	Disp. (km)	Fault Name	Disp. (km)
1	MCT	204.4	MCT	161.3	MCT	161.3	Same as Api Flex 3		MCT	220.5	Same as Simikot Flex 1	
2	RT 1	47	RT 1	50.05	RT 1	50.05			RT 1	205.83		
3	RT 2	138.3	RT 2	143.5	RT 2	143.5			RT 2	56.95		
4	LHD 1	22.5	LHD 1	29.1	LHD 1	29.1			RT 3	51.6		
5	LHD 2	22.5	LHD 2	25	LHD 2 (partial)	17.5			RT 4	48.48		
6	LHD 3	21.1	LHD 3	25.38	OOST 2	6.9			RT 5	10.69		
7	LHD 4	39.1	LHD 4	38.05	LHD 2 (full)	7.5			LHD 1	51.2		
8	LHD 5	3	LHD 5	3.7	LHD 3	25.38			LHD 2	36.82		
9	LHD 6	22.5	OOST 1	5.31	LHD 4	38.05			LHD 3A	9.5		
10	SHTS 1	17.2	LHD 6 (partial)	20	LHD 5	3.7			LHD 3B	30.7		
11	SHTS 2	12	Normal 2	-1.7	OOST 1	5.31			LHD 4	37.65		
12	SHTS 3	15	Normal 3	-3.5	Normal 4	-2.2			LHD 5	31.8		
13	Normal 1	-1.5	LHD 6 (full)	7	LHD 6 (partial)	18.5			LHD 6	16.15		
14	Normal 2	-5.3	SHTS 1	15	Normal 2	-3.5			SHTS 1	1.29		
15	Normal 3	-6.4	SHTS 2	12.78	Normal 3	-1.7			SHTS 2	22.83		
16	OOST 1	4.3	Normal 1	-2.6	LHD 6 (full)	8.5			SHTS 3A	8.41		
17	Normal 4	-4.8	SHTS 3	14.95	SHTS 1	15			LHD 7	7.51		
18	OOST 2	10.5	Normal 4	-2.2	SHTS 2	12.78			OOST	2.6		
19			OOST 2	6.9	Normal 1	-2.6			SHTS 3B	9.5		
20					SHTS 3	14.95			SHTS 4	15.44		

MCT = Main Central Thrust, RT = Ramgarh Thrust and related Lower Lesser Himalayan Faults, LHD = Lesser Himalayan Duplex related horse faults, SHTS = Sub-himalayan Thrust System related faults, Normal = Normal slip fault, OOST = Out-of-sequence thrust fault. See corresponding figures for Api and Simikot cross sections for fault traces.

Table 2. Flexural Model Kinematic Sequences

3.3 AGE CORRELATION AND SUBSIDENCE CURVES FROM NON-STATIC (MODELED) LOADS

Finally, with a complete flexural and isostatically modeled cross section, that exhibits the full deformation and subsidence of the system, it is possible to create a subsidence curve (e.g. DeCelles and Giles, 1996; DeCelles, Gehrels, Quade, and Ojha, 1998; Xie and Heller, 2009) at a higher level of detail than previously possible. However, this is possible only if, in addition to the model geometry through time, each step in the model can be correlated to a specific age in the deformational history. In the Himalayas, several paleomagnetic studies have been conducted in stratigraphic profiles near both of the sections modeled in this study (Ojha et al., 2000, 2009; Guatam and Fujiwara, 2000) and the high temporal and vertical resolution of the pseudo-stratigraphy in this method allows the two to be correlated (e.g. Fig. 2). Subsidence curves in particular are created by extracting the curvature of a horizon at a specific step in the model and determining the maximum depth of the basin at that time at a specified point. For this study we use the location of the lower cutoff point of the MFT for both sections.

4.0 RESULTS

The following results include models, which do not match available geologic constraints. These models (specifically Api Flex 1 and 2, and Simikot Flex 1) are shown to illustrate the iterative process leading to a best-fit solution. This process is three-fold: (1) the flexural model is conducted repeatedly with systematically varying flexural parameters (EET, Density, and erosion angle α) until the isostatic wavelength and decollement angle produce a match close to that inferred from observations, (the geology at the surface, the depth of the foreland basin and decollment dip), (2) once a general flexural solution is found, the kinematic order is adjusted to produce a chronological and stratigraphic match to the erosion of key units and their deposition in the foreland, respectively, and (3) in this study the models were conducted both with and without sediment loading, which requires different flexural parameters (a lower EET and separate rock/sediment densities) but maintains the same kinematic order. In this research, this process required evaluating 23-29 models for both sections in order to systematically refine all possible variables.

4.1 API SECTION

The original Api section (Robinson et al., 2006, Fig. 4a) proposed three OOS thrusts and two normal faults. Due to a lack of temporal constraints, the original kinematic restoration of this section (Robinson, 2008) placed these faults at the end of the kinematic sequence (thus most recently in time), which is likely unrealistic. 18 model iterations were conducted without sediment loading and 5 with sediment loading in order to fine-tune the flexural parameters in both cases systematically. Through modeling we propose a new, more reasonable kinematic order, and show a selection of successful and unsuccessful models in order to illustrate the iterative process

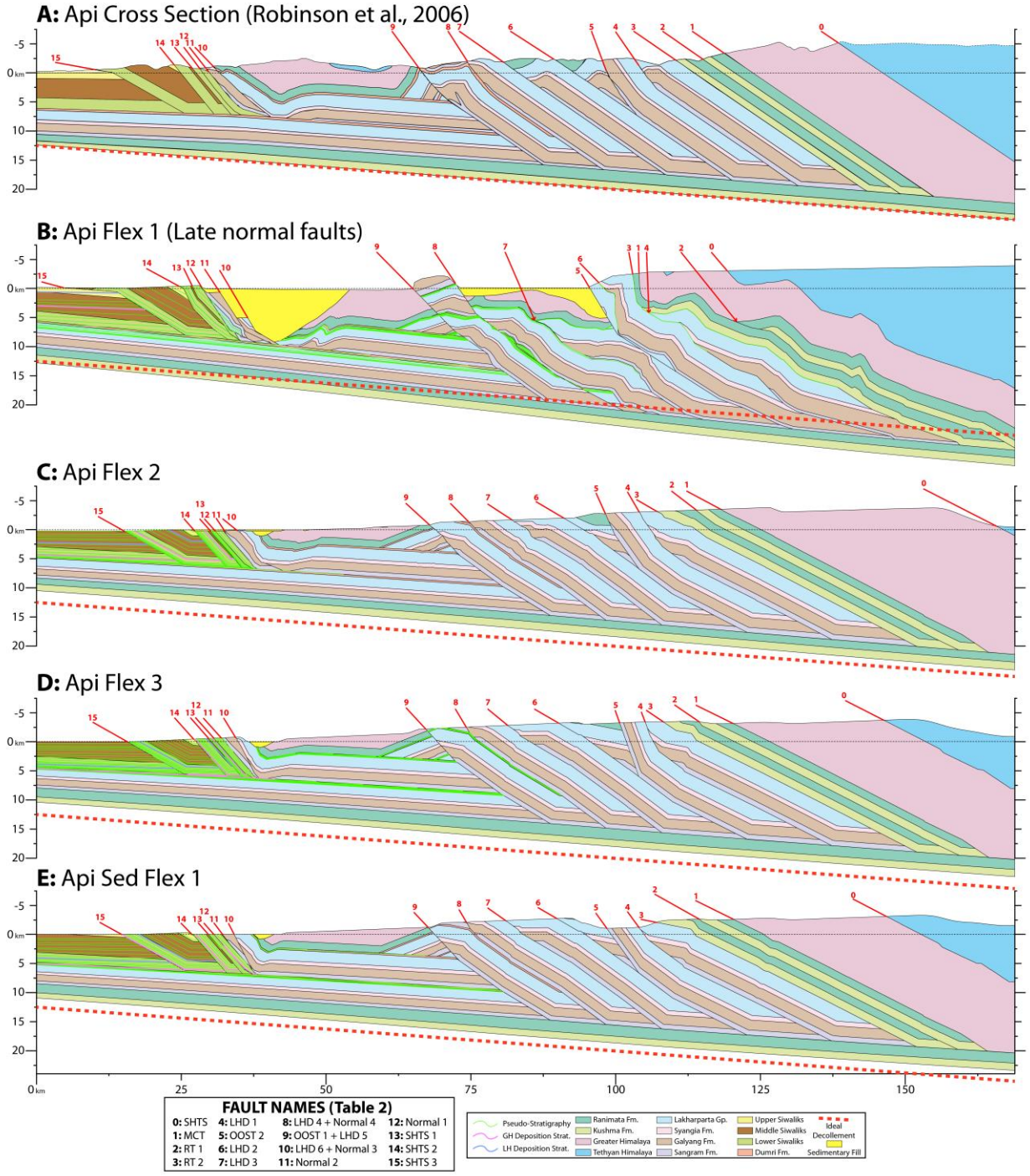

Figure 4. Comparison of modeled results with the original section from Robinson, 2006 (A). Final model results from Api Flex 1-3 (B-D) and Api Sed Flex 1 (E). (See Table 1 for model flexural parameters and fault line names correspond to those in table 2.)

4.1.1 Api Flex 1: Api Model with Late/Modern Normal Faults (e.g. Robinson, 2008)

The kinematic order used in this model, which was identical to that proposed by Robinson (2008), resulted in a final configuration which is markedly inconsistent with modern observations (Fig. 4b). The late normal faults created an intermontane basin that was 30 km wide and up to 10.5 km deep (Fig. 4b). In addition, the low EET (65 km) and high bulk rock density (2800 kg/m^3) utilized in this model created a steep decollement angle (5.1-6.3º). The resulting excessive depth of the hinterland (+7 km) caused erosion of the GH to occur very late in the model, which conflicts with provenance data showing it occurred much earlier. GH detritus was deposited at a depth equivalent to the Middle Siwalik member. LH deposition occurred so late that its deposition was not preserved in the MFT sheet. Thus the primary problems with this model are flexural parameters, which produce a steep decollement and too much subsidence, and the extreme normal fault basin that indicates that normal faults in this section cannot have occurred recently.

4.1.2 Api Flex 2: Api Model with Revised Kinematic Order but Mismatching Pseudo-stratigraphy

Another kinematic and flexural model (Api Flex 2, Table 1, Fig. 4c), used both a higher EET (80 km) and a lower density (2650 kg/m^3) and the initial stratigraphy was lowered 0.75 km with respect to sea level to prevent erosion of the exposed Lakharparta formation due to passage of the forebulge. Additionally, the kinematic sequence was revised such that normal and thrust OOS faults occurred earlier in the chronology in order to avoid the creation of a normal fault basin and allow more realistic scenarios for OOS fault motion as a response to sub or super-

critical taper conditions (see Table 2 for kinematic sequence). While these parameters produced a reasonable decollement angle between 4.3-4.8º and additionally yielded a surficial geology that matched the exposed surface geology, the deposition and erosion of the GH and LH occurred very late in the model progression (Fig. 4c and Table 1) such that GH detritus was deposited in the lower Siwalik (0.95 km above the MFT) and LH detritus deposited near the base of the Upper Siwaliks (5.26 km above the MFT). Provenance data suggest that this modeled erosion simply occurred too late, either due to early subsidence in the hinterland or, again, inaccurate kinematic sequence for OOS faults.

4.1.3 Api Flex 3: Api Model with Revised Kinematic Order and Best Fit Flexural Parameters (Without Sediment Loading)

To correct the depositional and erosional sequence of the model, the kinematic order was again revised with most OOS faults occurring at the earliest possible stage geometrically permissible. Adjusting the flexural parameters with increased EET (90 km), increased bulk density (2750 kg/m^3) and about the same α angle (Api Flex 3, Table 1, Fig. 4d) allowed GH material to be eroded and deposited within the Dumri formation as indicated by provenance data. Additionally, the most hinterlandward OOS thrust was placed such that it occurred during early development of the LHD, which allowed LH material to be eroded significantly earlier than previous models, and to thus be deposited at an appropriate depth in the Siwlaik Group (Fig. 4d). The final result adequately matched most parameters (surficial geology, decollement angle, and provenance indicators); however the overall depth of the decollement was about 1 km too shallow from the hinterland to the foreland, meaning that while the flexural wavelength may be

acceptable (producing an adequate decollement angle between 4.18-4.26º) the overall load was too low.

4.1.4 Api Sed Flex 1: Api Model with Revised Kinematic Order and Best Fit Flexural Parameters (With Sediment Loading)

The final flexural and kinematic model for the Api cross section used an additional sediment loading step and once again adjusted flexural parameters (Api Sed Flex 1, Table 1, Fig. 4e). The goal was to evaluate the effect of the sediment load on the modeled basin history, and to more accurately account for the load distribution through time. The best fit model with sediment loading required a bulk rock density of 2500 kg/m^3 and sediment density of 2300 kg/m^3 with an EET of 70 km. The result matched the mapped surface geology, decollement angle, and foreland basin depth as well as the deposition (depth and thickness) and erosion of key provenance signals.

In detail, the modeled LH detritus was deposited at a stratigraphic thickness of 1.79 km measured perpendicular to bedding above the MFT at the lower cutoff of the fault, this is at nearly the same thickness as the measured Lower-Middle Siwalik transition accounting for 0.8 km of unexposed Lower Siwaliks. This modeled thickness corresponds well with the negative shift in εNd at 1.7-2.3 km above the MFT (Robinson et al., 2001), which spans both the top of the Lower Siwalik and the base of the Middle Siwalik. GH deposition in this model occurs ~0.2 km above the MFT measured from the bottom cutoff of this fault. This is at the base of the Lower Siwalik Mbr. – not the Dumri Fm., as suggested based on provenance studies which show plagioclase grains in the Dumri Fm. at Dumri Bridge (DeCelles, Gehrels, Quade, and Ojha, 1998; Robinson et al., 2001). However, while the occurrence of plagioclase is compatible with

GH detritus, it does not require GH rocks to be the source. At Khutia Khola, the first observation of kyanite and sillimanite grains (and thus crystalline GH detritus) occurs within the Lower Siwaliks at ~1.5 km above the MFT, (DeCelles, Gehrels, Quade, Ojha, et al., 1998)., GH erosion in our preferred model occurs after 331 km of displacement with erosion through GH material overlying the core of the growing LHD. The exposed material was originally buried 15-20 km at the start of the model (Fig. 3a), a sufficient depth for kyanite and sillimanite formation. The pseudo-deposition of this GH material occured at a depth of 5.6 km (.8 km above the MFT) (Fig. 2a). Finally, while a normal fault related basin remains within the final model, its dimensions are minimal (only 3.51 km wide by 0.78 km deep), and exists in a region with limited direct geologic observations (DeCelles et al., 2001; Robinson et al., 2006). The closest strike and dip observation is ~7 km to the west. With these factors in mind, we argue that this model produced the most accurate final result in the Api section.

4.1.5 Age Correlations and Deformation Rate

The depths of the pseudostratigraphy and associated time steps of the Api Sed Flex 1 model were correlated to a measured paleomagnetic stratigraphy section in the region of Khutia Khola (Ojha et al., 2000), which is directly adjacent to the trace of the Api section (Fig. 1, < 5 km east). This paleomagnetic section covers a ~ 2400 m vertical stretch of Siwalik Group rocks uplifted and exhumed by the MFT, but neither the base or top of the sheet was observed. As such, correlations were made assuming the LS-MS contact as the anchor point between the paleomagnetic section and that inferred by field mapping (Robinson et al., 2006), and thickness correlations were made below and above this point (Fig. 2a). Correlation of deformation steps to measured age allows the calculation of shortening rates between steps or series of steps in the

flexural model. Key OOS fault steps from this model and the modeled topographic angle (□) are shown in Fig. 5. Deformation rates calculated for each of the model steps are shown in Table 3 and Fig. 6. The initial start date of 25 Ma is the starting age of the model, based on the oldest observed $^{40}Ar/^{39}Ar$ cooling age in the GH (Robinson et al., 2006). Three versions of correlations were created: (1) Table 3a and the green curve in Fig. 6 shows correlations to the Khutia Khola section alone, assuming that all other data was too distant to be reliably compared, (2) Table 3b and the orange curve in Fig. 6 shows the correlations of Khutia Khola combined with interpolated correlations to both the Swat Khola paleomagnetic stratigraphy (Ojha et al., 2009), and that at Karnali River (Guatam and Fujiwara, 2000) in order to illuminate parallel pulses in deformation, and (3) Table 3c is a partial alteration to the data in Table 3b where normal fault slip (calculated as negative displacement) is ignored in the full displacement estimates. Considering Table 3b and the orange curve in Fig. 6, the end date of step range 1-7 at 20.9 Ma is an estimation of the depositional age of the base of the Dumri located in far western Nepal. The measured age at the base of the Dumri (19.9 Ma) reported in a paleomagnetic study at Swat Khola (Ojha et al., 2009) is ~ 200 km to the east near the Simikot Section. We proposed that the base of the Dumri is older at Api because the restoration length is shorter than Simikot, meaning the flexural basin will reach the Dumri location earlier. Proposed ages for steps 17-19 are based on correlations to the Karnali River paleomagnetic stratigraphy of the LS and MS near Simikot (Guatam and Fujiwara, 2000). Steps 20 through 26 are the steps correlated to the paleomagnetic stratigraphy of the Khutia Khola section (Ojha et al., 2000). Step range 27-33 is constrained by the ages of the MS-US contact, which is not exposed in Khutia Khola. The age of the MS-US contact in the corresponding Simikot thrust sheet at Karnali, must be younger than 5 Ma (Guatam and Fujiwara, 2000), and is measured to be between 2.5 and 3.5 Ma in western Nepal

and between 3.0 and 3.5 Ma in central Nepal (Ojha et al., 2009). An estimated 2.5 Ma start of Upper Siwalik deposition at Api suggests rates of deformation from 2.5 Ma to present are 19.45-20.5 mm/yr, similar to modern geodesy rates (19±2.5 mm/yr, Bettinelli et al., 2006) and Holocene rates based on warped river terraces (21.5±2 mm/yr, Lavé and Avouac, 2000). The proposed shortening rates are determined by dividing displacement amount at each step or over each step range in the model by the estimated age of that displacement based on our correlation between the modeled pseudostratigraphy and the measured magnetostratigraphy.

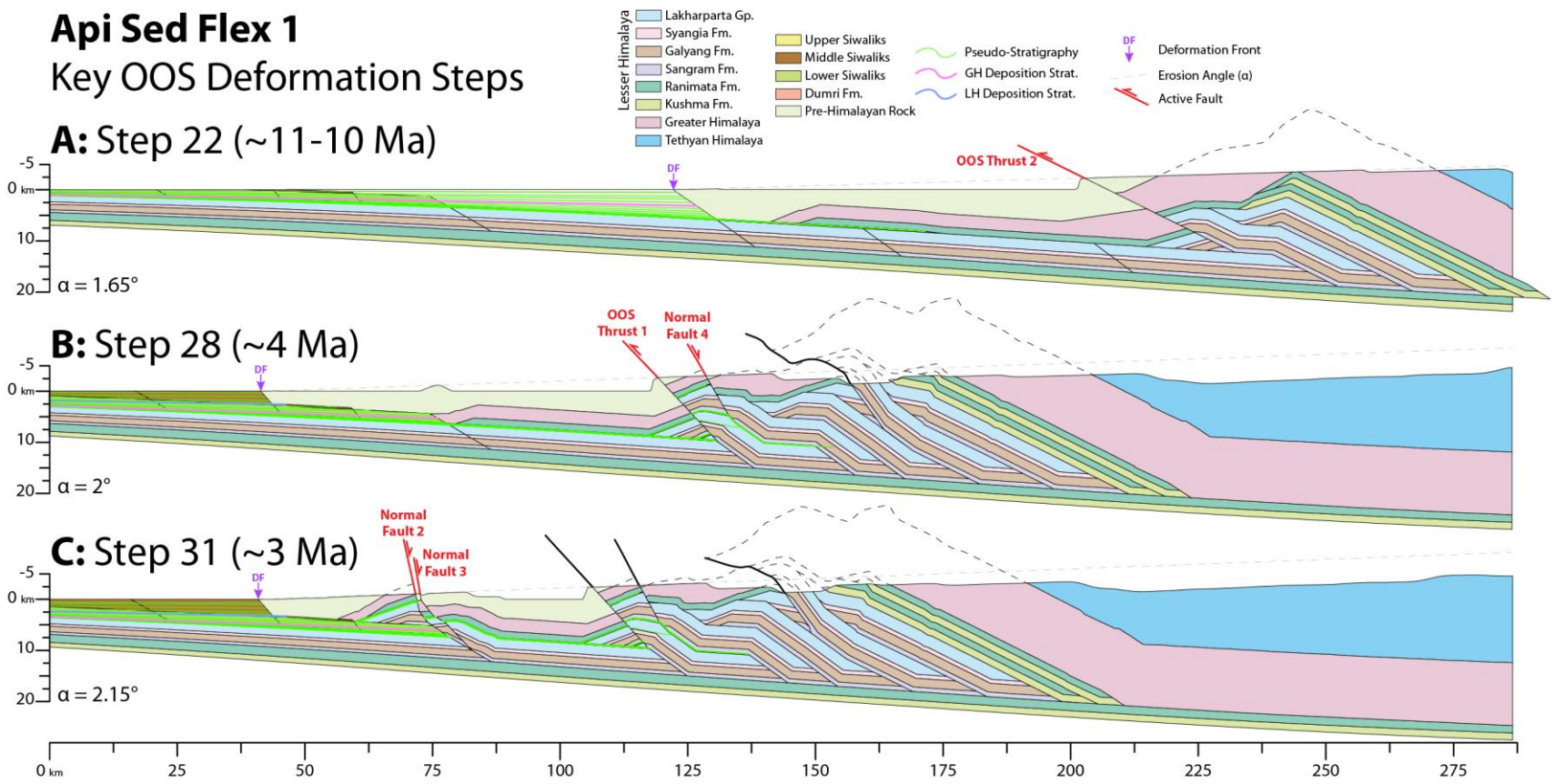

Figure 5. Key deformation steps in Api Sed Flex 1 – the best fit Api model. (fault names from Table 2)

API AGES AND SHORTENING RATES (with interpolation from Simikot)

Model Step/Range	Unit	Fault	End Age	Displacement	Shortening Rate	NOTES
			25			<- Model start age.
1-7	Dumri	MCT	20.9	140	34.15	
8	Dumri	MCT-RT	20.3	21.3	35.50	
9	Dumri	RT	19.28	20	19.61	
10	Dumri	RT	18.45	15.025	18.10	<- Ages interpolated from Swat Khola.
11-12	Dumri	RT	17.05	35.025	25.02	
13	Dumri	RT	16.7	20	57.14	
14-16	Dumri	RT	15.7	60	60.00	
17	D-LS	RT	15.35	20	57.14	<- Age of LS Depo from Karnali R.
18-19	LS	RT-LHD	14.7	38.05	58.54	<- Approx. Age ~0.5 km above MFT.
20	LS	LHD	13.3	14.55	10.39	
21	LS	LHD	11.9	17.5	12.50	
22-23	LS	LHD	10.77	14.4	12.74	<- Ages come from the Khutia Khola correlations (Ojha 2000).
24	LS-MS	LHD	9.7	12.69	11.86	
25	MS	LHD	8.5	12.69	10.58	
26	MS	LHD	6.7	19.025	10.57	
27-30	MS	LHD	4.1	25.835	9.94	
31-33	MS-US	LHD	2.5	13.3	8.31	<- Approx. age of US depo.
34-38	US	LHD-SHTS	0	48.63	19.45	<- Present day.

B

TOTAL DISPLACEMENT:	AVERAGE RATE IF CONSTANT:
548.02	21.92

API AGES AND SHORTENING RATES (with only available data)

Model Step/Range	Unit	Fault	End Age	Displacement	Shortening Rate	NOTES
			25			<- Model start age.
1-20	D-LS	MCT-RT-LHD	14	383.95	34.90	
21	LS	LHD	12.4	17.5	10.94	
22-23	LS	LHD	11	14.4	10.29	<- Ages come from the Khutia Khola correlations (Ojha 2000).
24	LS-MS	LHD	9.75	12.69	10.15	
25	MS	LHD	8.6	12.69	11.03	
26	MS	LHD	6.8	19.025	10.57	
27-33	MS-US	LHD	2.5	39.135	9.10	<- Approx. age of US depo.
34-38	US	LHD-SHTS	0	48.63	19.45	<- End of model, 0 Ma.

A

TOTAL DISPLACEMENT:	AVERAGE RATE IF CONSTANT:
548.02	21.92

API AGES AND SHORTENING RATES (Simikot interp. w/o normal faults)

27-30	MS	LHD	4.1	28.035	10.78	
31-33	MS-US	LHD	2.5	18.5	11.56	<- Approx. age of US depo.
34-38	US	LHD-SHTS	0	51.23	20.49	<- Present day.

C

TOTAL DISPLACEMENT:	AVERAGE RATE IF CONSTANT:
558.02	22.32

Table 3. Shortening rates for Api Sed Flex 1. (A) Api rates of shortening using only immediately available data in close proximity to the Api section (at Khutia Kohla). (B) Api rates of shortening if age correlations from Simikot (in the Swat Khola and Karnali River sections) are interpolated 150 km to the west at Api. (C) Api rates of shortening if Simikot interpolations are made and normal fault displacements (which are negative, decreasing the full displacement) are omitted.

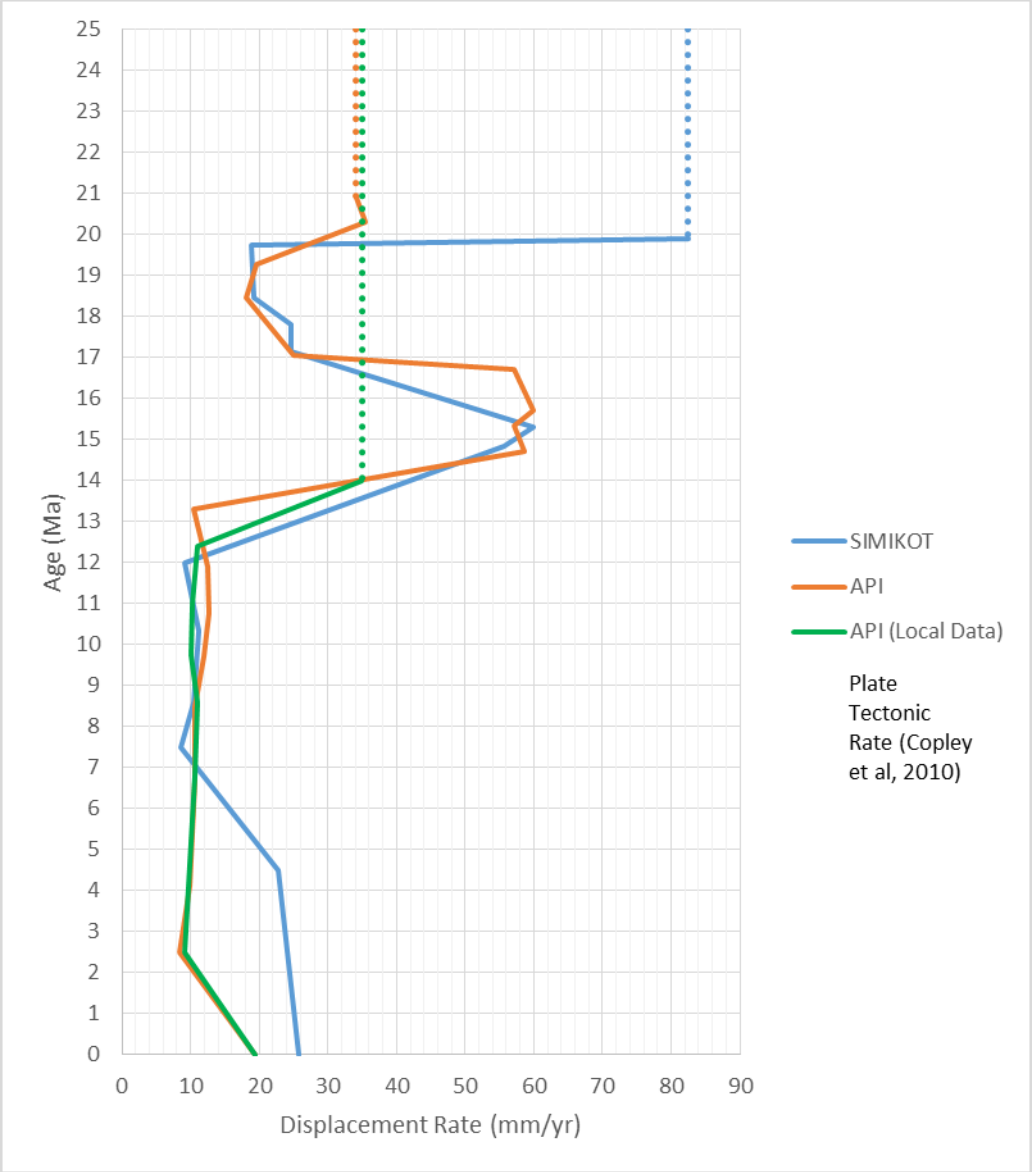

Figure 6. Displacement rate as a factor of age in the Simikot and Api sections. "Local data" signifies that the ages in this curve were calculated only for data immediately local to the Api Section at Khutia Kohla and not interpolated over from Karnali River or Swat Kohla.

4.2 SIMIKOT SECTION

The Simikot section used in this study is a reinterpretation of the Robinson et al. (2006) original cross section (Fig. 7a). This section was modified to account for the presence of active uplift documented near the MCT trace in the hinterland and immediately south of the Dadeldhura Klippe in the south (Harvey et al., 2015). The major changes include: (1) Sub-Himalayan Thrust System faults now follow a more listric path based on additional strike and dip measurements that call for changes in the fault angle (i.e. from 45 º to ~30 º dips, Robinson et al., 2006; Mugnier et al., 1998, 1999), (2) the addition of an active ramp underneath the Main Boundary Thrust sheet, as proposed by Harvey et al. (2015) as a mechanism for active uplift south of the klippe, (3) modification of the hinterlandward LH duplex such that the OOS thrust only cuts through the full thickness of one thrust sheet and has a more reasonable fault trace (more gradually dipping with a ramp at ~55º and flat at 27º, as opposed to a full decollement-to-surface ramp at 60º), and (4) no minor OOS thrust is required to repeat Bhainskati and Dumri formations directly adjacent to the Main Boundary Thrust, instead there is an in-sequence thrust repeating these units. As with Api, this section was modeled both with and without the sediment loading step.

The restored Simikot section, measured from MFT to the ramp of the MCT, is a full 337 km longer than the restored Api section. Because of this, the flexural wavelength must be large to cause adequate subsidence in the foreland. There are two ways to reproduce this necessary wavelength: (1) the EET must be very high (100+ km, which causes less subsidence where the load is focused but also a wider distribution of the load weight, or (2) the load itself must be

more widely distributed, which can be accomplished by accounting for the sediment load. With this in mind, both means of increasing the flexural wavelength were tested, and 13 models without sediment loading were conducted, and 16 with sediment loading, until the parameters were systematically refined to provide the best possible match.

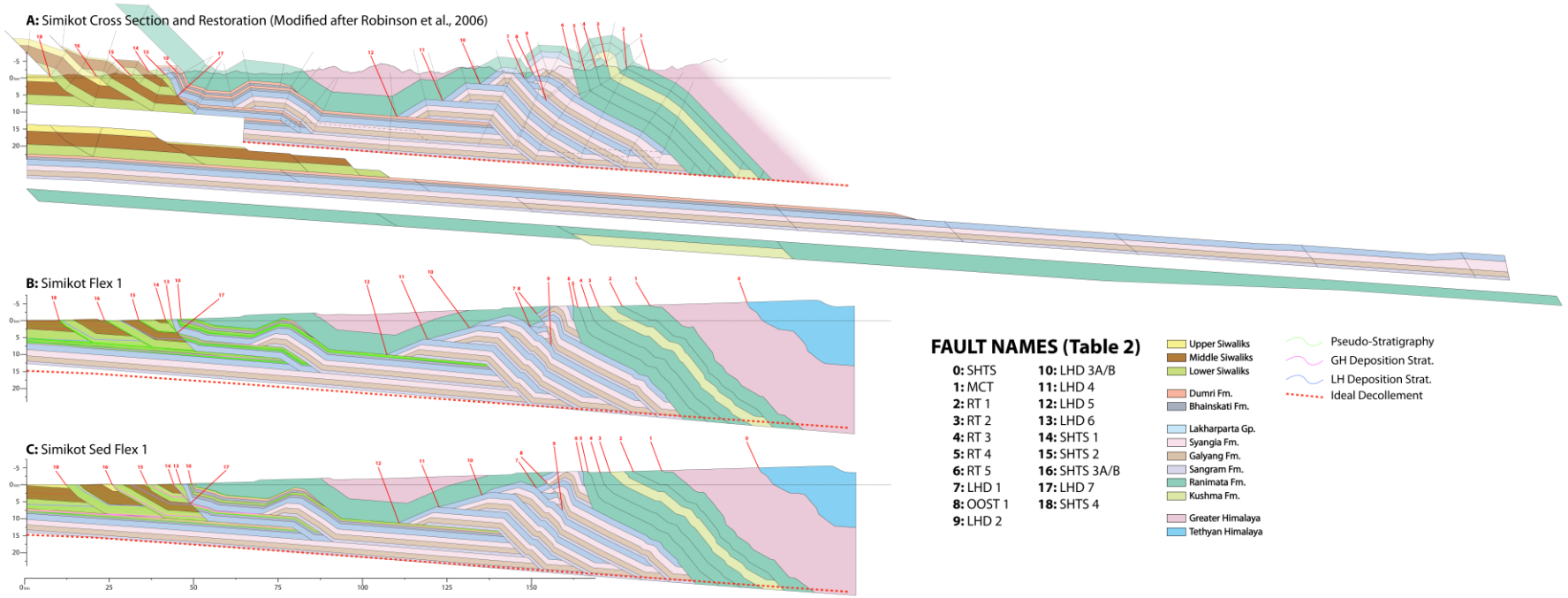

Figure 7. (A) New interpretation of Robinson et al., 2006's Simikot cross section with full palinspastic restoration, (B) Simikot Flex 1 final model, (C) Simikot Sed Flex 1 final model. Fault names correspond to names in Table 2.

4.2.1 Simikot Flex 1: Simikot Model with High Parameters and Closest Possible Fit (Without Sediment Loading)

Initial modeling of the Simikot section was performed without sediment loading, the closest possible match we attained is shown in Fig. 7b. This model used a bulk rock density of 2850 kg/m^3 with an EET of 100 km and a constant α of 1.6° throughout the model. This model still retains some critical mismatches to the surficial geology. The hinterland is a good match to the surface and proposed subsurface geology with a decollement at the appropriate depth (~31 km at its deepest point) but, due to inadequate subsidence in the foreland, the southern surficial geology and faults are misaligned by ~2.6 km due to over erosion and the foreland basin is too shallow (~ 2 km). The correct level of erosion in the hinterland combined with too much erosion in the foreland is a function of a decollement angle that is up to 2° too steep because the EET is too low and thus the flexural wavelength is too narrow. A similar model was conducted with a rock density of 2950 kg/m^3 and resulted in an even steeper decollement angle, a foreland basin that was only 1 km too shallow, but a hinterland that was 3 km too deep. An EET of 100 km is the highest possible value allowed by the MOVE software. We hypothesize that an EET of 105 km or 110 km and a density of 2900 kg/m^3 would provide a sufficient load distribution to match the depth of the foreland, decollement angle and surface geology.

4.2.2 Simikot Sed Flex 1: Best overall fit Simikot Model (With Sediment Loading)

The best overall fit for the Simikot section was achieved only by the addition of sediment loading to the model process (Simikot Sed Flex 1, Table 1, Fig. 7c). Using a bulk rock density of 2500 kg/m^3 and sediment density of 2300 kg/m^3 with an EET of 95 km, enough subsidence was produced in the foreland to deposit the full stratigraphic (8.8 km thick) Siwalik Group section. The difference in thickness between the Simikot Siwalik section (8.8 km), and the Siwalik section measured at Khutia Khola (6.2 km) complicates direct depth comparisons between the two sections. Instead, we discuss the relative position of provenance indicators within the modeled stratigraphy. In the Simikot model, GH material was eroded early enough to be deposited 0.8 km below the MFT at its lower cutoff point, placing it squarely within the Dumri Fm. The LHD was breached after 719 km of displacement in the system and deposited at a thickness of 4.4 km above the MFT, within the lower quarter of the Middle Siwalik unit. While again this thickness differs from the 1.7-2.3 km thickness for LH εNd signal (Fig. 2a) found by Robinson et al. (2001) at Khutia Kohla, it does fit the age of a negative shift in εNd for stratigraphy near the Karnali River (location in Fig. 1, stratigraphy and provenance shown in Fig. 2b) (Szulc et al., 2006).

As previously described, the Simikot section geometry was revised in order to co-locate the previously mapped OOS fault (Robinson et al., 2006) with geomorphic indices of active uplift (Harvey et al., 2015) (Fig. 7a and 8). Additionally, we relocated the LHD footwall ramp northward to this location to overlap with the OOS thrust and thus reflect one centralized zone of uplift. The OOS thrust is required due to the mapped contact of the Upper LH Syangia Formation faulted over the lower LH Ranimata Formation. Unlike the Api section, where early OOS faults helped expose LH rocks at the appropriate times, LH rocks in the Simikot section did

not need additional uplift and erosion to match the provenance record in the foreland. However, late activation of OOS thrusts facilitated a match between the uplift proposed in the model to the northern zones of active uplift related observed by Harvey et al. (2015).

The second, southern physiographic transition zone, PT2-S, (representing active uplift) observed by Harvey et al. (2015) is also represented in the model by a new active ramp directly beneath the southernmost outcrop of the MCT (See Fig. 7a and 8). Just as with PT2-N, the two most likely methods to explain this may be either an additional OOS fault, or uplift from a deeper in-sequence fault ramp. We have interpreted this zone to be caused by an in-sequence ramp, which cuts through the upper three LH formations, Lakharparta, Bhainskati, and Dumri, but which also exhibits partial OOS motion in order for the hanging wall of this ramp to be emplaced on top of the northern most Sub-Himalayan Thrust System thrust. Thus, together, both zones are accounted for by OOS and in-sequence motion that agrees both with the geologic map (Robinson et al., 2006) and the geomorphology of the region. Kinematically, motion on both OOS thrusts on the northern thrust and southern ramp occurs two displacement steps before the final step of the models, which is approximately < 2 Ma before present (Table 2, Simikot Sed Flex 1, LSD 7 and OOST 1).

4.2.3 Age Correlations and Deformation Rate

As with the Api section, correlations were made between dates derived from paleomagnetism and the modeled pseudostratigraphy (Fig. 2b). In addition to paleomagnetic stratigraphy of the Siwalik Group (Guatam and Fujiwara, 2000), a similar study was conducted on the outcrop of the Dumri Formation located near Swat Khola (Ojha et al., 2009). These correlations together provide age constraints of modeled deformation steps back to 19.9 Ma, the

measured basal age of the Dumri. The ages and rates derived are shown in Table 4 and the blue curve in Fig. 6. As with the Api section, 25 Ma is, the assumed start of MCT deformation (Robinson et al., 2006). Steps 1-20 are constrained by the Swat Khola measurements (Ojha et al., 2009). A slight age gap exists between the top of the measured Dumri Formation dated to ~16-15.3 Ma (Ojha et al., 2009) and an established LS chron at 15.1 Ma (Guatam and Fujiwara, 2000). Thus we use a LS depositional age of 15.3 Ma. Steps 27-31 are directly correlated to the Guatam and Fujiwara measurements (2000), and finally step range 32-35 is estimated to be 4.2 Ma assuming a diachronous deposition of US sediment between Simikot and Api due to differences in thickness. A 2.5 Ma start to US deposition would argue for rates twice as fast as modern rates from 2.5 Ma to present.

SIMIKOT AGES AND SHORTENING RATES

Model Step/Range	Unit	Fault	End Age	Displacement	Shortening Rate	NOTES
		MCT	25			<- Model start age.
1-17	Dumri	MCT-RT	19.9	420.5	82.45	
18	Dumri	RT	19.75	2.83	18.87	<- Ages come from Swat Khola correlations (Ojha 2009).
19	Dumri	RT	18.45	25	19.23	
20	Dumri	RT	17.8	15.975	24.58	
21	D-LS	RT	17.15	15.975	24.58	
22-26	LS	RT	15.3	110.77	59.88	
27	LS	LHD	14.85	25	55.56	
28	LS	LHD	12	26.2	9.19	<- Ages come from the Karnali River correlations (Guatam).
29	LS	LHD	10.35	18.41	11.16	
30	LS-MS	LHD	8.6	18.41	10.52	
31	MS	LHD	7.5	9.5	8.64	
32-35	MS-US	LHD	4.5	68.35	22.78	<- Approx. Age of US depo.
36-45	US	LHD-SHTS	0	115.53	25.67	<- Present day.
				TOTAL DISPLACEMENT:	**AVERAGE RATE IF CONSTANT:**	
				872.45	34.90	

Table 4. Shortening rates for Simikot Sed Flex 1. Certain ages correlated to the Karnali River paleomagnetic stratigraphy (Guatam and Fujiwara, 2000).

5.0 DISCUSSION

5.1 OOS FAULTS AND THEIR KINEMATIC ORDER AS INFERRED FROM FORWARD MODELING: THE PSEUDO-STRATIGRAPHY METHOD

5.1.1 Api Section Kinematic Order

The flexural modeling performed in this study has allowed us to propose a new, more precise, relative kinematic sequence solution for the Himalayan belt in far western Nepal. In the Api section we interpret much of the OOS faulting to have occurred at the earliest possible time for each fault, given cross cutting relationships. For instance, OOS Thrust 2 – with 6.9 km of displacement – in the best-fit models Api Flex 3 and Api Sed Flex 1 (Table 2) occurs after partial displacement on the second LHD thrust, which allows the trace of OOS Thrust 2 to follow the path of the underlying ramp (Fig. 5a), thus requiring less energy to initiate faulting (e.g. Mitra and Boyer, 1986). This early OOS motion allows the LH stratigraphy to be unroofed and eroded at a much earlier time – and thus to be deposited at an appropriate depth in the foreland (Table 1), than if the thrust occurred later in the model. Continuing forward, OOS Thrust 1 (The Arnakoli thrust, e.g. Robinson, 2008) occurs after displacement on the fifth LHD thrust, with again just enough displacement such that the OOS thrust is able to break through the overriding sheet following the path of the in-sequence thrust ramp. However, the preceding LHD thrust (the

fifth thrust in the duplex) causes significant stacking of thrust material. While it is easier for OOS thrust 1 to occur after this stage (Fig. 5b), the OOS uplift of material in this stack invokes a very steep topographic angle and brings the system to a super-critical state. To compensate for this change, we argue that Normal Fault 4 occurs immediately after motion on OOS Thrust 1. While it may seem contrary for a normal fault to occur right after thrusting, if the critical state of the system is considered, it is logical for compensation of the super-critical wedge angle to occur in order to return the system to a critical state (Dahlen et al., 1983, 1984; Morley, 1988). Additionally, as with the other normal faults, this prevents the preservation of a basin associated with Normal Fault 4, as seen in the final result of Api Sed Flex 1 (Fig. 4e) between 70 and 90 km N-S distance. The sixth LHD thrust carves off a significantly longer horse (51 km) than any preceding thrust (40-44 km) propagating the locus of uplift southward. The deformation front, however, does not propagate forward from where it had been during LHD thrust 5 because it is pinned at the northern extent of the more recent Sub-Himalayan Thrust System zone. Without any adjustment, pinning the deformation front would cause the immediate topographic angle (α) to increase up to 7-8º. To compensate for this super critical state, we argue normal fault 2 and 3 occur after partial displacement of the sixth LHD thrust (Fig. 5c), to allow α to return to ~2.15º without a dramatic increase in erosion rate. This is again a situation where normal faulting occurs in close kinematic order to thrust motion. The overall motion on these normal faults totals 5.2 km, which causes significant lowering of topography immediately to the north. We propose that this is the best possible kinematic order given the fault geometry of our starting cross-section. However, a different fault geometry (that still matches the map data) or a different kinematic sequence may still produce a more mechanically feasible solution.

This order of events for deformation in the Api section provides matches to the following key observations: (1) surficial geology produced by the model is in close agreement with that mapped and presented in Robinson et al. (2006) (Fig. 4e) and the only normal fault basin preserved is of small enough dimensions (up to 0.78 km deep, 3.5 km wide) and in an area not yet directly mapped and potentially is yet to be undocumented, and (2) erosion and deposition events of both GH and LH material, due to the breaching of the MCT sheet and the LHD respectively, agree with all provenance indicators recorded in the foreland of Khutia Khola (DeCelles, Gehrels, Quade, Ojha, et al., 1998; Robinson et al., 2001) – GH material is deposited within the Lower Siwalik unit (where kyanite and sillimanite are first observed, DeCelles, Gehrels, Quade, Ojha, et al., 1998), and LH detritus is modeled in the lower quarter of the Middle Siwalik unit (where εNd values become more negative, Robinson et al., 2001). While other kinematic solutions may be possible for this region, They would require a significant alteration of the geometry of the cross section to match the known surface geology, and foreland basin constraints.

5.1.2 Simikot Section Kinematic Order

With the exceptions of the two OOS thrusts and additional LH ramp near to the Main Boundary Thrust, the kinematic order of the Simikot section (Table 2) is similar to that presented by Robinson (2008). The absence of normal faults in the cross section simplify the refinement of the kinematic sequence (no normal fault basins were produced). Instead, the geomorphologic and seismic indicators of active uplift serve as the primary chronologic proxy for the OOS thrusts (Harvey et al., 2015). Therefore, late activation on the two thrusts exhibiting OOS motion was preferred, and the faults were activated after 837 km of displacement in the system, a stage

which is approximately dated between 2.5 and 1 Ma (Table 4). In addition to the OOS thrusts, the double footwall ramps proposed in our new cross section serve to both enhance any uplift signals in the location of PT2-N and PT2-S (Fig. 8) and extend the duration of uplift to the Holocene as all material in the section must travel over these ramps. As shown in Fig. 8, the proposed ramps are in direct alignment with the Physiographic Transitions and seismic clusters observed along this section, something which other sections through the same region do not match (Fig. 8 and DeCelles et al., 2001; Berger et al., 2004; Robinson et al., 2006). However, while this solution has the potential to explain these observations, more work is necessary to fully confirm this proposed geometry. Specifically, thermokinematic modeling of the revised fault geometry (e.g. McQuarrie and Ehlers, 2015, 2017) in the Simikot model will allow cooling age patterns to be compared with measured observations. Additionally, the indicators of active uplift – sharp contrasts in river steepness, knick points, and perched/relict topographies (e.g. Kirby and Whipple, 2012) – which were observed by Harvey et al. (2015) should be present at the new locations of proposed active uplift. This may be tested through incorporating a dynamically eroding and evolving topography. More detailed landscape and topographic modeling such as merging the cross section kinematics into a planform landscape model such as CASCADE (Braun and Sambridge, 1997) would be able to show whether or not this proposed cross section geometry reproduces geomorphology akin to that observed by Harvey et al. (2015).

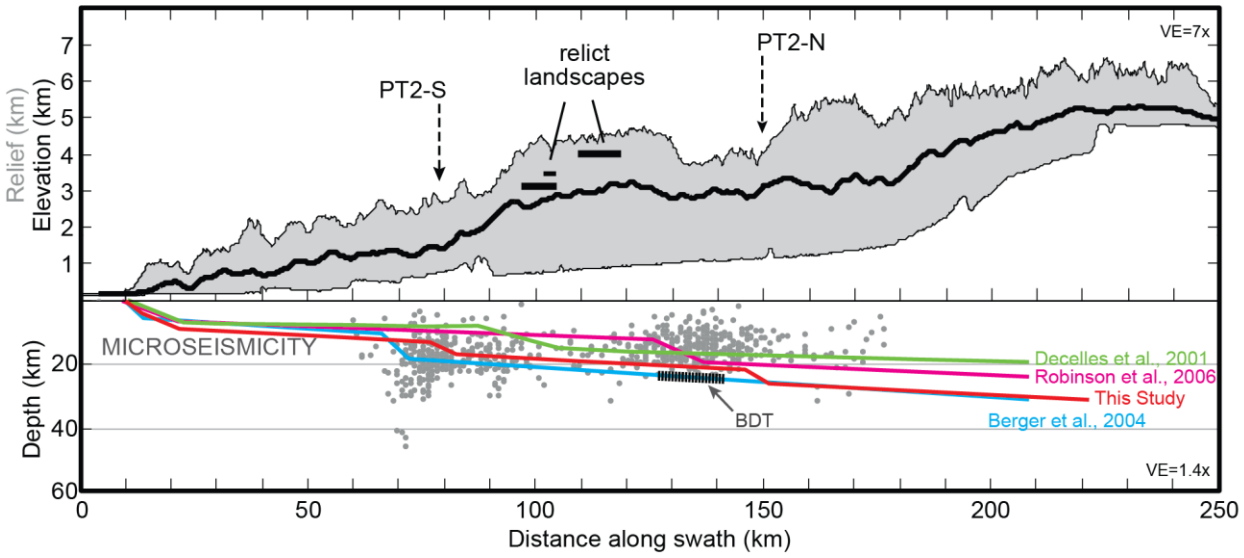

Figure 8. Topographic swath, decollement geometry, and seismic foci along the Simikot Section. Note how the decollement ramps from the cross section in this study pair with the Physiographic Transitions and the seismic clusters. (After Harvey et al., 2015)

5.1.3 Dating of incremental thrust fault displacement

A discussion of the shortening rates determined via these models must begin with the noticeably fast shortening rate of the MCT at ~82 mm/yr calculated between 25 and 19.9 Ma in the Simikot section (Table 4, Fig. 6). Although previous research has supported variable (and fast) displacement rates in the Himalaya through time (Kohn et al., 2004; Long et al., 2012; Robinson and McQuarrie, 2012; Tobgay et al., 2012), we recognize that this calculated rate is faster than Indian-Asian plate convergence at this time (45-50 mm/yr between 25-20 Ma, Copley et al., 2010). We cannot explain away this discrepancy and instead propose two viable solutions which could lessen the extreme shortening rate: (1) The thickness of the repeating Ranimata Fm. exposed in the Lower LH duplex is unknown (Robinson et al., 2006). The thickness of the Ranimata Fm., assumed by Robinson et al. (2006) to be the same as that exposed to the north,

could be an underestimate of the true thickness. Thus instead of three thrust sheets, a permissible interpretation could be only two stacked sheets of Ranimata in this location, which would lessen the distance the forebulge would need to travel (by at least 50 km) and thus lower the shortening rate to ~ 70 mm/yr. (2) The assumption that MCT displacement begins at 25 Ma could be incorrect. The age is based on the cooling age of muscovite in GH rocks due to erosional exhumation which brought the rocks through the muscovite $^{40}Ar/^{39}Ar$ closure temperature between 25 to 21 Ma based on muscovite ages found in the Dadeldhura Klippe and GH rocks north of the MCT (Robinson et al., 2006; Antolín et al., 2013), permitting earlier motion on the MCT. It is possible that MCT motion started earlier than 25 Ma and that the MCT sheet material was not uplifted and exhumed to the proper depth and temperature till this time. To bring the displacement rate down to 50 mm/yr, the MCT would need to start deforming at 28 Ma. A combination of both approaches would bring MCT shortening down to 50 mm/yr with initiation of deformation at 27 Ma.

Continuing forward, shortening rates of the RT, and lower LH duplex at ~24-18 mm/yr between ~19.75 to 14.85 are reasonable rates in comparison to modern GPS displacement rates (Bettinelli et al., 2006), and within the range of rates determined via similar flexural modeling at ~27-14 mm/yr (Robinson and McQuarrie, 2012). However, our proposed rates increase again, up to 55-60 mm/yr, between ~17.8-14.85 Ma. Because the southern most thrust sheet that carries the Ranimata Formation sheet moves during this time, this high rate may also be a result of too much displacement. Alternatively, this could be a window of time of rapid shortening of the fold-thrust belt in far western Nepal. Previous studies have suggested periods of shortening at or above plate tectonic rates in the Himalaya albeit over different windows of time. Using Th-Pb isotopic dating of monazite Kohn et al. (2004) suggested that the Ramgarh thrust moved at ~ 70 mm/yr

from 10.5 to 8.9 Ma in central Nepal. A similar study in western Bhutan argued for 40-60 mm/yr rates between 20 and 15 Ma (Tobgay et al., 2012; McQuarrie et al., 2014). Rapid shortening rates (70 mm/yr) in eastern Bhutan are proposed for a narrow window of time between 12 and 8 Ma (Long et al., 2012; McQuarrie and Ehlers, 2015) with very slow shortening rates (7-10 m/yr) both preceding and post-dating the window of rapid shortening. In far western Nepal along the Simikot section shortening rates drop significantly to 10-8 mm/yr, between 12-7.5 Ma, during primary construction of the LHD. Rates increase to modern values of 20-27 mm/yr between 4.2 Ma to the present.

Table 3b and the orange curve in Fig. 6 shows the rates at Api with correlations interpreted from the Simikot paleomagnetic stratigraphy. This was done in an attempt to align the rates at Api to those calculated at Simikot (Table 4 and Fig. 6). If we interpret the basal age of the Dumri Fm. in the Api Section to be 20.9 Ma (older than the 19.9 Ma age at Simikot from Swat Kohla because of the narrower flexural wave and earlier deposition at Api), then from 25-20.9 Ma, the MCT displaces at an average rate of 34 mm/yr. This difference in rate is again based on the significant difference in shortening magnitudes between the two sections during MCT and RT displacement. Again, using Simikot as an example, if the initiation of displacement on the MCT was as early as 27 Ma, (to decrease the MCT rate at Simikot) the rate between 27-20.9 Ma at Api would decrease to ~22 mm/yr. A 26 Ma MCT start would permit a rate of ~27 mm/yr. Thus, the noted difference in shortening between the two sections may also point to slight diachroneity between the Api and Simikot MCT activation periods. The age of the base of the Lower Siwalik unit is again interpolated from the Karnali paleomagnetic section near Simikot to be 14.7 Ma, which yields a similar rate for early RT displacement at 19-25 mm/yr (vs. 18-24 mm/yr at Simikot.) The transition from RT displacement to the start of development of the

LHD may also be characterized by another jump in shortening rate to 60-57 mm/yr between 17.05-14.7 Ma, paralleling the 55-60 mm/yr rate at Simikot between 17.15-14.85 Ma. This rate is not required by Api data alone and without the Simikot correlation the longer-term rate from 25 to 17.7 Ma is 34 mm/yr (average rate for the MCT, RT, and beginning LHD) (Table 3a and Fig. 6). During LHD development the rate falls to 10 mm/yr between 14.7 and 13.3 Ma, the same as at Simikot at a parallel time range of 14.85-12 Ma, and increases up to a maximum of 12 mm/yr at 10.77 Ma, and back down to 8.3 mm/yr until 2.5 Ma. In contrast to Simikot, there is not enough shortening in the last portion of the model to increase shortening rates between 7.5 to 2.5 Ma. This is partially due to the presence of normal faults, which provide negative slip. Table 3c shows the final rates of Api to be 3-4 mm/yr higher if these normal faults are not considered. From 2.5 Ma to the present the rate is calculated to be 19 mm/yr, agreeable to modern GPS rates (Bettinelli et al., 2006).

5.1.4 Creation of subsidence curves via modeled subsidence and comparison to flexural calculations

The subsidence curve for Simikot (Purple curve in Fig. 10) is created by measuring the depths imposed by the flexural wave throughout the model at the modern location of the basal MFT cutoff point (~12 km north of the outcrop of the MFT in this section.) Points of measurement used in the curve throughout the model are based on when syn-tectonic sedimentary units are first deposited (i.e. the Dumri, and all three members of the Siwalik Group.) The curve was extrapolated beyond 19.9 Ma (the age of the passage of the forebulge) by plotting a line from the model at step 17 (19.9 Ma) that extends ~330 km south of the MFT. This line has experienced the full flexural load from 25 Ma to 19.9 Ma and thus represents the flexural

wave of the model parameters. This curve is shown in Fig. 10 with both distance and age, plotted assuming a 20 mm/yr average displacement rate throughout the model. Alongside this curve are the calculated flexural curves for a 3 km high, 125 km half width load with a density of 2650 kg/m^3. The modeled flexure assumes a sediment density of 2400 kg/m^3, a mantle density of 3300 kg/m^3, and flexural rigidity, D, that varies from 1.0e24 to 7.0e24 (equivalent to an EET between 54-104 km, respectively.) These were calculated using the equations of Turcotte and Schubert (1982) for a rectangular load on an unbroken plate. It is clear that the magnitude of the modeled subsidence curves do not match the calculated curves. The vertical maximum predicted subsidence is a function of the size of the load (larger load equals greater subsidence). In addition, unlike the static load curves, the modeled curves are the result of a model with a dynamically evolving load and associated incremental flexural response (Fig. 9). As discussed in section 3, the modeled loads are the integral result of a flexural wavelength calculated repeatedly for a dynamically evolving load of precise, non-rectangular dimensions through time. Static flexural curves assume a load approximately equal to the modern topography the Himalaya. In contrast, the modeled load equals the load imparted by all material uplifted above the topography of the previous step. After the load adjusts, then the remaining material above the new projected topography is removed and the associated rebound due to the erosion of that material is calculated. This incremental increase (the load that precedes erosion) indicates that the true load for a system will always be larger than the preserved topography. The higher load permits a deeper foreland basin, (increasing the amplitude of the basin) (as shown in Fig. 9 for 6 example model steps) without changing the wavelength.

Unlike the amplitude of the subsidence, which is driven by the size of the load, the wavelength of the curve is set by the flexural rigidity, thus comparing the modeled dynamic to

static curves, the location and extent of the forebulge becomes the critical parameter for comparison. Based on the wavelength over the forebulge, the Simikot curve can be paired with a calculated curve between D = 4.6e24 and D = 7.0e24 (or EET between 90-104 km) which is consistent to the 95 km EET used in the Simikot model (Simikot Sed Flex 1, Table 1). Additionally, this analysis of the model agrees with the observation of DeCelles et al. (2004) that places the 49-45 Ma Bhainskati Formation (Najman et al., 2005) as the backbulge of the flexed Indian margin. Both the calculated flexural curves and the modeled curves predict backbulge sedimentation over at least this time span assuming a 20 mm/yr average migration rate (Fig. 10). Although our models predict back bulge sedimentation prior to 40 Ma, they are limited by two factors: (1) our models do not start until at least 25 Ma and thus do not experience flexural loading earlier than this, and (2) the horizontal extent of the modeled flexural wave is not long enough to cover the full extent of the backbulge. In light of these caveats, the similarity of our modeled flexure to the static model wavelength suggests maximum backbulge deposition between 45-43 Ma.

Comparison of the modeled subsidence curve for Api (Blue curve in Fig. 10) to calculated ones shows that it's wavelength is longer than D = 2.2e24 (EET = 70 km) but less than 4.6e24 (EET = 90 km), which is acceptable given the EET used in this model was 70 km.

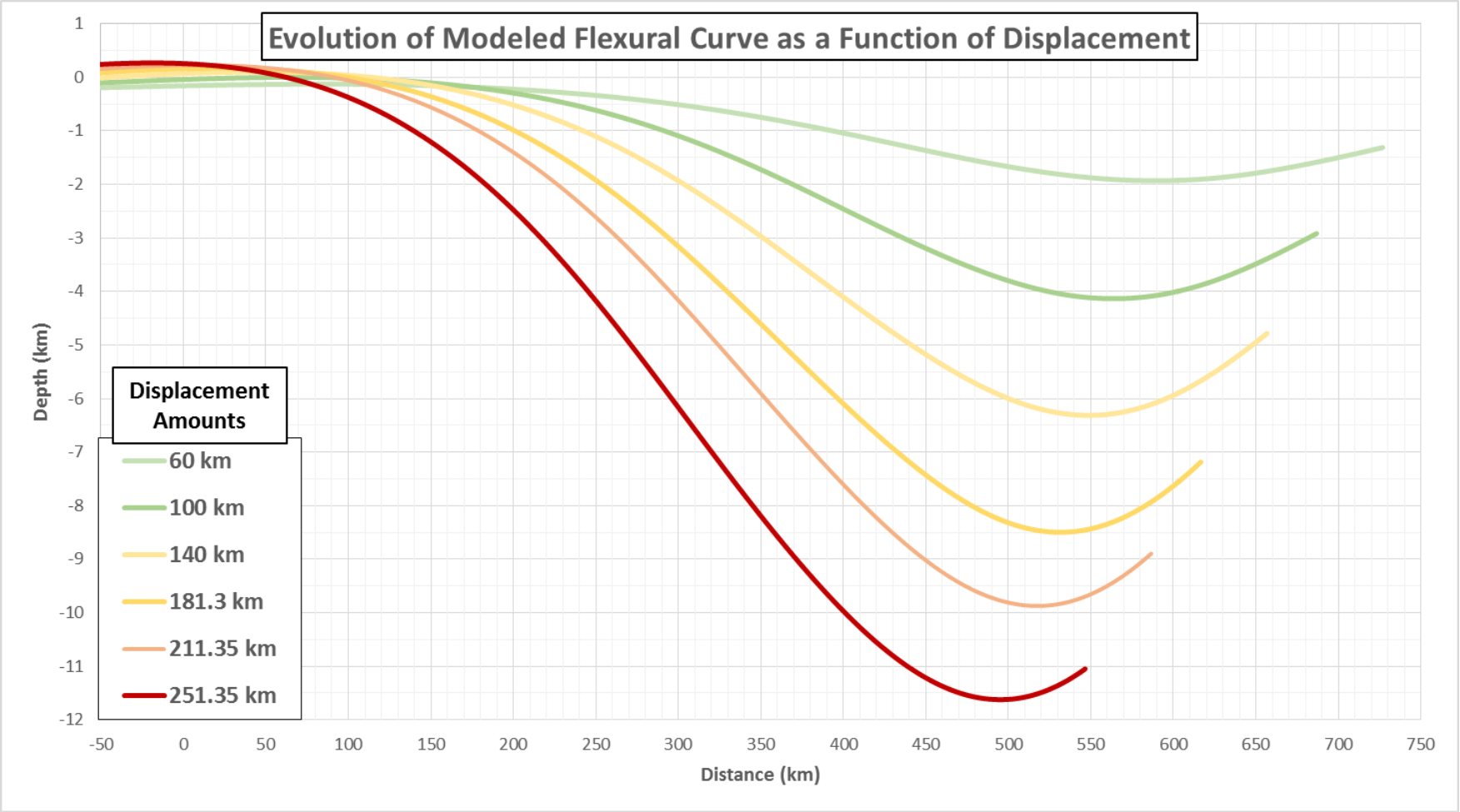

Figure 9. Evolution of the modeled flexural curve through time in the model as a function of displacement amount at six different time steps in the Api Sed Flex 1 model. Note how the flexural wavelength shifts to the left but does not lengthen overall, instead wave amplitude increases significantly due to progressive loading.

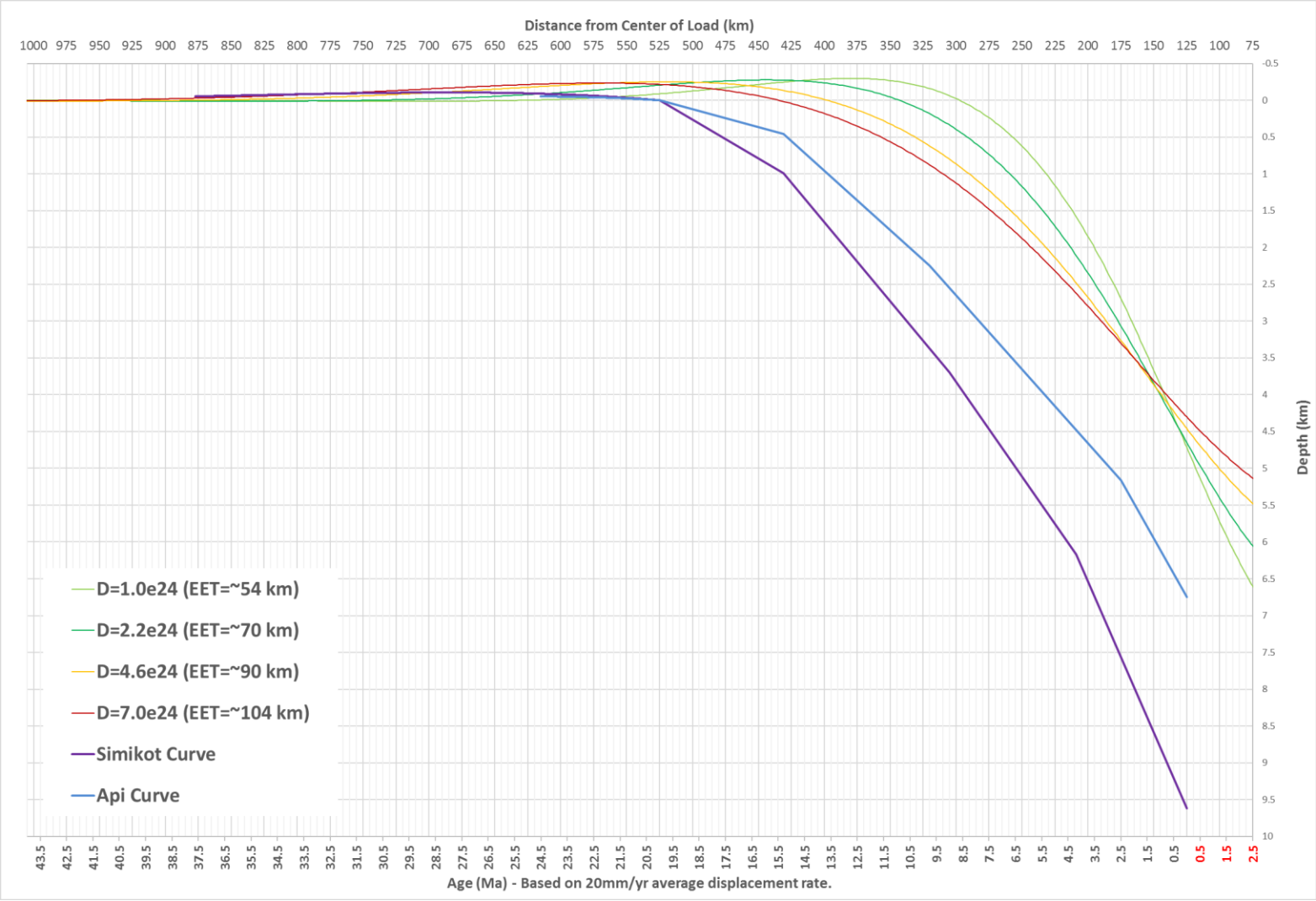

Figure 10. Subsidence curves for Api (Api Sed Flex 1) and Simikot (Simikot Sed Flex 1) compared to calculated flexural curves for varying Flexural Rigidities and the following parameters: Load Height = 3 km, Half-width = 125 km, Rock density = 2650 kg/m^3, Sediment density = 2400 kg/m^3, Mantle density = 3300 kg/m^3, g = 9.8 m/s^2

5.1.5 Discrepancies in provenance studies between Api and Simikot

The provenance studies between Api and Simikot, which are used in this study to constrain the deformation and kinematic sequence, have some marked dissimilarities that provide insight into variations in structure. Szulc et al. (2006) observe provenance at three separate locations, one along the Karnali River, and the remaining two, Surai and Tinau, both, ~150 km eastward of Karnali and Simikot). They note that carbonate detritus is observed at about 12 Ma in the Karnali section could possibly be LH derived. However, while Szulic et al. (2006) point to the Khutia Khola εNd values described in Robinson et al. (2001) as showing a decrease to more negative εNd values also at 12 Ma, they do not actually observe values low enough to equate to a significant detrital contribution of LH material (~-17) at Karnali until 6 Ma, which places it within the lower third of the Middle Siwalik unit (Guatam and Fujiwara, 2000). In our modeled basin response, Simikot Sed Flex 1, LH deposition occurs in step 33, which is between 7.5 and 4.5 Ma, consistent with the εNd value measured in the Karnali section. At Khutia Khola (Api) this measured negative shift occurs between 10-8.5 Ma (Robinson et al., 2001), which similarly spans the lower quarter of the Middle Siwaliks (Ojha et al., 2000). Api Sed Flex 1 has LH deposition occurring in step 23, which is dated between 11-10.77 Ma. The different age for when LH material enters the basin (between the Api section and Simikot) argues against lateral continuity of tectonic evolution, unroofing, and deposition through the Central Himalayas suggested by Szulc et al. (2006). Our modeling of the provenance data from the Khutia Khola and the Karnali River section supports a West-to-East progression of unroofing, as concluded by Robinson et al. (2001), and logically makes sense considering the modern areal exposure of LH rocks exposed in the west of Nepal vs. the east (Fig. 1a.) Thus, while the modeled provenance

for LH detritus at Simikot (Fig. 2b) does not match the depth or age of modeled LH dertritus in the MFT sheet at Api (Fig. 2a), both independently match the provenance data and age available for each section.

The stratigraphic level and age of GH detritus entering the foreland basin is also different between the two sections. Opposite to the LH detritus variations, we note that, at Khutia Khola (Api), the first appearance of Kyanite and Sillimanite indicative crystalline GH material is within the Lower Siwalik unit (DeCelles, Gehrels, Quade, Ojha, et al., 1998), while at Dumri Bridge (~200 km east of Api and ~150 km east of Simikot, Fig. 1) the Dumri Formation contains increased plagioclase and detrital zircon ages closely related to material derived from the GH (DeCelles, Gehrels, Quade, Ojha, et al., 1998) indicating exposure much earlier in the deformation sequence. While Dumri Bridge is eastward of the Simikot section, the sample location within the LH thrusts is comparable to where the Dumri outcrops along the Simikot section. The difference between the key GH detrital indicators from these two locations (Khutia Khola and Dumri Bridge) match the modeled differences of when the GH gets erosionally exhumed suggesting there was likely an East-to-West progression of GH exhumation, where Simikot exhibits deposition of GH detritus within the Dumri (Fig. 2a), at Api this same provenance indicator is within the Lower Siwalik Unit (Fig. 2a).

Provenance and stratigraphic studies are critical tools in the interpretation of kinematic evolution in fold and thrust belts, as long as lateral differences are acknowledged and the studies being correlated to modeled results are in close physical proximity to the cross section being modeled. As shown in this study, they can be used to refine the temporal resolution of kinematic events in cross sections, such as OOS faults and the shortening rate through time. Additionally, this flexural and erosional forward modeling method utilizing modeled pseudo-stratigraphy can

illuminate potential errors in the geometry of the section, as in the case of duplex geometry at Simikot as well as the geometry and magnitude of frontal (southern) normal faults at Api.

5.1.6 Impact of Provenance Correlation and Sediment Loading on Flexural and Erosional Forward Models

Comparing the results of Api Flex 2 to Api Flex 3 (Table 1), we note that Api Flex 2 did not produce an accurate foreland provenance signal, and that erosion events occurred at different stages in the displacement (GH erosion occurred at 370 and 331 km of displacement, LH at 481 and 415 km in Api Flex 2, and Api Flex 3, respectively) and thus both produced vastly different provenance and erosion histories, but still resulted in almost the same surficial and subsurface geology (Fig. 4c and d). Specifically, in Api Flex 2 GH erosion occurs after 370 km of displacement and is deposited ~1 km above the MFT in the Lower Siwaliks, which is slightly higher than the same event in Api Flex 3 (in which GH detritus occurs at 0.2 km above the MFT in the Lower Siwaliks) and thus is ~1.5 km lower than the first observed appearance of kyanite and silimanite at Api (DeCelles, Gehrels, Quade, Ojha, et al., 1998). However, LH erosion in Api Flex 2 does not occur until 481 km of displacement. At this time, motion on OOS Thrust 1 (Table 2) causes ~3.6 km of focused erosion through the MCT and underlying LHD facilitating deposition of LH detritus in the upper quarter of the Middle Siwaliks at ~5 Ma, a marked contrast to the 10-11 Ma age of the εNd LH signal (Robinson et al., 2001). In Api Flex 3, OOS Thrust 2 (the more hinterlandward OOS thrust) occurs early in the model, after only 408 km of displacement and causes ~5 km of erosion through GH rocks, but does not immediately erode LH material. Continued slip over the ramp on the underlying horse (415 km of displacement) causes ~3 km of erosion. This breaches the LHD and deposits LH detritus ~1.5 km above the

MFT, correlative to the measured signal recorded in the lower portion of the middle Siwaliks at ~11.7 Ma. Thus, the Api Flex 2 model is objectively wrong, but would not be visible without provenance data. The location and magnitude of erosion, which provides constraints on the kinematics of a cross section, are discernable either through basin provenance data or a thermochronometric model of the kinematics, which would identify a predicted a cooling history which did not match observations (e.g. McQuarrie and Ehlers, 2015). The significant difference between Api Flex 2 and 3 is the order of out of sequence faults (Table 2), which causes the erosion of LH material earlier in Api Flex 3 and Api Sed Flex 1 due primarily to OOS Thrust 2. We thus hypothesize that Api Flex 3 would produce a more accurate cooling history and require less model revision to achieve this match than Api Flex 2.

The difference between Api Flex 3 to Api Sed Flex 1 (Table 1), is much more subtle. Both models had the same magnitude of erosion occurring at the same stages in the deformation (GH erosion occurs at 331 km of displacement, LH at 415 km in both models) but that detritus deposition occurred at slightly different depths in the foreland (Table 1). The difference between these models is of course the modeling of sediment load. Discrepancies between the provenance depths alters the correlation of these model steps to stratigraphic ages, modifying interpreted model step ages. Specifically, looking at the deposition of LH detritus in both models, both are caused by continued slip of the duplex up to 415 km of displacement after motion on OOS Thrust 2 at 408 km, but; (1) in Api Flex 3, LH deposition occurs at a depth (~1.5 km above the MFT) which can be correlated approximately to ~11.7 Ma, (2) in Api Sed Flex 1, the LH deposition depth is ~1.7 km above the MFT and is correlated to an age of ~10.7 Ma. The difference in depth (and thus difference in age) is due to including the sediment load in the flexural model. Thus, another important observation from this study is that flexural and erosional

forward models are made more robust when a separate sediment load is included in the modeling process. It is important to note however, including a sediment load did not notably alter the erosional history of the model (since erosion still occurs at the same deformation steps, and is the same magnitude). In some cases, though, like Simikot, the only viable and realistic model result is achieved through the integration of a sediment load – however this is due to the extreme length of the palinspastic restoration (~880 km), which requires a similarly long flexural wavelength. As shown with the non-sediment load model (Simikot Flex 1), it is impossible for our modeling process to have a thrust only load that provides the subsidence necessary to match deposition on the foreland. While simplified loading processes can still produce a valid kinematic model, if provenance is going to be used as a proxy for kinematic history as in this study, we recommend that sediment loading is taken into account for increased accuracy. Additionally, if sediment loading is proven to be necessary for a model to match (as in Simikot), then it may illuminate errors in the geometry and require the cross section to be revisited and reconsidered.

Finally it must be pointed out that the flexural parameters used in these models are non-unique, the value of densities, EETs, and topographic angles are flexible and changes in one parameter require changes in all others in order to provide a match. For instance, while we have used a constant EET for our models, EET may increase through time (e.g. DeCelles, 2012) due to progressive rigidity of the underlying craton. Even with this caveat, if the model produces a match to all available data including the provenance, it is an accurate description of the kinematic, erosional and depositional history (as in Api Flex 3 and Api Sed Flex 1, Table 1), which is the critical goal of any model.

6.0 CONCLUSIONS

The model results presented in this paper are what we propose to be valid and permissible solutions to the geometry, kinematic order, and dynamic flexural response of a linked fold-thrust belt- foreland basin system through time. In the Api section, the most important finding is that OOS faults make a vast difference in both the final surficial geology and the foreland provenance record. Most noticeably, if normal faults are proposed in the kinematic history of a cross section, then they must be correctly ordered in any kinematic sequence such that they do not produce egregious basins, which are not preserved in the geology today (as in Api Flex 1). Less noticeably, OOS thrusts may have an unusually significant effect on the provenance signal. Due to their highly vertical component of motion, these faults have the unique ability to enhance uplift and erosion and thus have a considerable effect on subsequent depositional signal. We argue that the OOS thrusts in the Api section occurred between ~11 Ma (OOS Thrust 2) up to ~4 Ma (OOS Thrust 1/Normal Fault 4) and that the final normal faults occurred synchronously with in-sequence thrust motion at ~3 Ma in order to avoid the preservation of basins. In the Simikot section, the most important observation illuminated through this research is that geomorphological proxies for fault activity and can be used to govern the kinematic order and geometric configuration of a cross section. Because of the zones of geomorphic transition observed by Harvey et al. (2015), we propose that the two OOS thrusts in this section (Fig. 7) occurred simultaneously much later in the kinematic history than any OOS faults at Api, and can

be dated at least between 4.2 Ma to the present but may be as young as 2-1 Ma. This agrees with geomorphic indicators of active uplift along observed physiographic transitions. Importantly, the active footwall ramps in our revised Simikot model facilitate modern uplift highlighted by the geomorphology (Fig. 8). Additionally, in-sequence deformation of the section was sufficient in itself to produce the desired foreland provenance indicators without the added uplift of OOS faults.

The displacement rates calculated for the Api section range from 9-35 mm/yr only if the immediately available sedimentary data is considered (Table 3a, green curve in Fig. 6) but can also be shown to exhibit similar variations in displacement rate as seen in the Simikot section if correlations from Karnali and Swat Kohla are made (Table 3b/c, Fig. 6). Shortening rates calculated from the Simikot model model are shown to be extremely fast (Table 4, blue curve in Fig. 6) both during slip on the MCT (82 mm/yr) and at markedly fast at the end of the RT deformation (55-60 mm/yr). We suggest that an extra RT sheet may account for this discrepancy (Fig. 7, Table 2) and that two instead of three repeating LH thrust sheets would maintain the mapped surface contacts and geology (Robinson et al., 2006). This would decrease the total shortening in the Simikot section by 45-50 km and simultaneously decrease the expanse over which the flexural wavelength has to stretch to deposit the foreland basin and resulting pseudostratigraphy. A shorter section would also allow for a lower EET and density necessary to model the foreland basin. Thus, while flexural and erosional modeling has the potential to confirm new geometries based on geomorphic proxies, it also has the ability to highlight if a given geometry may be incorrectly interpreted. Considering the sections as a paired system due to their close proximity, we argue that the spikes and troughs in the pattern of displacement rate should be be consistent between the two sections and may indicate times of more rapid (or

sluggish) shortening in the region. This is similar to variations in displacement noted elsewhere in the Himalayas between 20-15 Ma (Tobgay et al., 2012; McQuarrie et al., 2014). Overall, the rates of faulting throughout both sections show a pulsed sequence of deformation rather than constant, as has been shown previously through similar, though less detailed flexural modeling (Robinson and McQuarrie, 2012).

We have shown through this research that sediment loading has an important effect on the flexural and erosional modeling process and the flexural parameters used, however the provenance match between Api flex 3 and Api Sed flex 1 indicates that a remarkably similar result can be obtained with and without modeling a sedimentary load – with discrepancies in age correlation of ~1 Ma, which is within error of most provenance studies. However, Api Flex 2 shows that while a model may reasonably match surficial geology available (Fig. 4), it may not match the provenance of the foreland (LH erosion did not occur until nearly the end of the model, ~5 Ma, Table 1). If there were no provenance data available, it would be impossible to argue that that model was incorrect, unless detailed cooling data were available (due to markedly different erosion histories). With provenance data, it is possible for models with and without sediment loading (Api Flex 3 and Api Sed Flex 1) to have erosional events occurring at the same stages of displacement, but measurable differences are observed in the deposition depth and thus the correlation and dating of deformation time steps (compare deposition depth of these models in Table 1). Thus detailed flexural modeling with provenance correlation has the potential to provide a first approximation of a kinematic sequence, thus requiring less model revisions to match the cooling history. Because of the discrepancy between the flexural parameters (Density/EET) used in sediment and non-sediment loading models, we do not cite the flexural parameters as final solutions to these values in the region.

Through this research we have shown that flexural and erosional forward modeling used in conjunction with foreland provenance information is a very useful tool in the creation of a detailed, dated kinematic history in which even OOS faults may be sequenced and dated, and geometries revised. This process may be broadly used in FTBs around the globe. The linkage of flexural and erosional modeling to stratigraphic studies facilitates the creation of a more detailed kinematic history through a cross section, which in turn can have implications for the broader understanding of plate tectonic history and how the partitioning of deformation along faults in a FTB system varies through time and space. If models such as these were conducted and synthesized for reconstructions across the whole Himalayan range, a diverse and detailed history of deformation and collisional tectonics in the region would emerge. However, all of this is only possible where detailed stratigraphic studies are readily available, thus adding value to that kind of research and integrating these disciplines to further understand the formation of mountains across the globe.

BIBLIOGRAPHY

Antolín, B., Godin, L., Wemmer, K., and Nagy, C., 2013, Kinematics of the Dadeldhura klippe shear zones (W Nepal): Implications for the foreland evolution of the himalayan metamorphic core: Terra Nova, v. 25, p. 282–291, doi: 10.1111/ter.12034.

Armstrong, F.C., and Oriel, S.S., 1965, Tectonic development of Idaho-Wyoming thrust belt: AAPG Bulletin, v. 49, p. 1847–1861.

Bally, A.W., Gordy, P.L., and Stewart, G.A., 1966, Structure, seismic data, and orogenic evolution of southern Canadian Rocky Mountains: Bulletin of Canadian Petroleum Geology, v. 14, p. 337–381.

Berger, A., Jouanne, F., Hassani, R., and Mugnier, J.L., 2004, Modelling the spatial distribution of present-day deformation in Nepal: How cylindrical is the Main Himalayan Thrust in Nepal? Geophysical Journal International, v. 156, p. 94–114, doi: 10.1111/j.1365-246X.2004.02038.x.

Bettinelli, P., Avouac, J.P., Flouzat, M., Jouanne, F., Bollinger, L., Willis, P., and Chitrakar, G.R., 2006, Plate motion of India and interseismic strain in the Nepal himalaya from GPS and DORIS measurements: Journal of Geodesy, v. 80, p. 567–589, doi: 10.1007/s00190-006-0030-3.

Boyer, S.E., and Elliott, D., 1982, Thrust systems: AAPG Bulletin, v. 66, p. 1196–1230, doi: 10.1306/03B5A77D-16D1-11D7-8645000102C1865D.

Braun, J., and Sambridge, M., 1997, Modelling landscape evolution on geological time scale: a new method based on irregular spatial discretization: Basin Research, v. 9, p. 27–52.

Bullen, M.E., Burbank, D.W., Garver, J.I., and Abdrakhmatov, K.Y., 2001, Late Cenozoic tectonic evolution of the northwestern Tien Shan: New age estimates for the initiation of mountain building: Bulletin of the Geological Society of America, v. 113, p. 1544–1559, doi: 10.1130/0016-7606(2001)113<1544.

Burchfiel, B.C., Zhiliang, C., Hodges, K. V., Yuping, L., Royden, L.H., Changrong, D., and Jiene, X., 1992, The South Tibetan Detachment System, Himalayan Orogen: Extension Contemporaneous With and Parallel to Shortening in a Collisional Mountain Belt, *in* Geological Society of America Special Papers 269, p. 1–41.

Butler, R.W.H., 1987, Thrust sequences: Journal of the Geological Society, v. 144, p. 619–634.

Cande, S.C., and Kent, D. V., 1995, Revised calibration of the geomagnetic polarity timescale for the Late Cretaceous and Cenozoic: Journal of Geophysical Research, v. 100, p. 6093, doi: 10.1029/94JB03098.

Castellarin, A., and Cantelli, L., 2000, Neo-Alpine evolution of the Southern Eastern Alps: Journal of Geodynamics, v. 30, p. 251–274.

Coleman, M.E., 1996, Orogen-parallel and orogen-perpendicular extension in the central Nepalese Himalayas: Bulletin of the Geological Society of America, v. 108, p. 1594–1607, doi: 10.1130/0016-7606(1996)108<1594:OPAOPE>2.3.CO;2.

Copley, A., Avouac, J.P., and Royer, J.Y., 2010, India-Asia collision and the Cenozoic slowdown of the Indian plate: Implications for the forces driving plate motions: Journal of Geophysical Research: Solid Earth, v. 115, p. 1–14, doi: 10.1029/2009JB006634.

Cruz, L., Malinski, J., Wilson, A., Take, W.A., and Hilley, G., 2010, Erosional control of the kinematics and geometry of fold-and-thrust belts imaged in a physical and numerical sandbox: Journal of Geophysical Research: Solid Earth, v. 115, p. 1–15, doi: 10.1029/2010JB007472.

Dahlen, F.A., 1990, Critical Taper Model of Fold-And-Thrust Belts and Accretionary Wedges: Annual Reviews of Earth and Planetary Sciences, v. 18, p. 55–99.

Dahlen, F.A., Suppe, J., and Davis, D., 1983, Mechanics of fold-and-thrust belts and accretionary wedges: Journal of Geophysical Research, v. 88, p. 1153–1172, doi: 10.1029/JB089iB12p10087.

Dahlen, F.A., Suppe, J., and Davis, D., 1984, Mechanics of fold-and-thrust belts and accretionary wedges: Cohesive Coulomb Theory: Journal of Geophysical Research, v. 89, p. 10087–10,101, doi: 10.1029/JB089iB12p10087.

Dahlstrom, C.D.A., 1969, Balanced cross sections: Canadian Journal of Earth Sciences, v. 6, p. 743–757, doi: 10.1139/e69-069.

DeCelles, P.G., Gehrels, G.E., Najman, Y., Martin, A.J., Carter, A., and Garzanti, E., 2004, Detrital geochronology and geochemistry of Cretaceous-Early Miocene strata of Nepal: Implications for timing and diachroneity of initial Himalayan orogenesis: Earth and Planetary Science Letters, v. 227, p. 313–330, doi: 10.1016/j.epsl.2004.08.019.

DeCelles, P.G., Gehrels, G.E., Quade, J., and Ojha, T.P., 1998, Eocene-early Miocene foreland basin development and the history of Himalayan thrusting, western and central Nepal: Tectonics, v. 17, p. 741–765, doi: 10.1029/98TC02598.

DeCelles, P.G., 2012, Foreland basin systems revisited: variations in response to tectonic settings, *in* Busby, C. and Azor, A. eds., Tectonics of Sedimentary Basins: Recent Advances, Oxford, Blackwell Publishing Ltd., p. 405–426.

DeCelles, P.G., Kapp, P., Ding, L., and Gehrels, G.E., 2007, Late Cretaceous to middle Tertiary basin evolution in the central Tibetan Plateau: Changing environments in response to tectonic partitioning, aridification, and regional elevation gain: Bulletin of the Geological Society of America, v. 119, p. 654–680, doi: 10.1130/B26074.1.

DeCelles, P.G., Gehrels, G.E., Quade, J., Ojha, T.P., Kapp, P.A., and Upreti, B.N., 1998, Neogene foreland basin deposits, erosional unroofing, and the kinematic history of the Himalayan fold-thrust belt, western Nepal: GSA Bulletin, v. 110, p. 2–21, doi: 10.1130/0016-7606(1998)110<0002:NFBDEU>2.3.CO;2.

DeCelles, P.G., Robinson, D.M., Quade, J., Ojha, T.P., Garzione, C.N., Copeland, P., and Upreti, B.N., 2001, Stratigraphy, structure, and tectonic evolution of the Himalayan fold-thrust belt in western Nepal: Tectonics, v. 20, p. 487–509.

DeCelles, P.G., and Giles, K.A., 1996, Foreland basin systems: Basin Research, v. 8, p. 105–123, doi: 10.1046/j.1365-2117.1996.01491.x.

Duncan, C., Masek, J., and Fielding, E., 2003, How steep are the Himalaya? Characteristics and implications of along-strike topographic variations: Geology, v. 31, p. 75–78, doi: 10.1130/0091-7613(2003)031<0075:HSATHC>2.0.CO;2.

Duvall, A.R., Clark, M.K., van der Pluijm, B.A., and Li, C., 2011, Direct dating of Eocene reverse faulting in northeastern Tibet using Ar-dating of fault clays and low-temperature thermochronometry: Earth and Planetary Science Letters, v. 304, p. 520–526, doi: 10.1016/j.epsl.2011.02.028.

Echavarria, L., Hernández, R., Allmendinger, R., and Reynolds, J., 2003, Subandean thrust and fold belt of northwestern Argentina: Geometry and timing of the Andean evolution: AAPG Bulletin, v. 87, p. 965–985, doi: 10.1306/01200300196.

Gansser, A., 1964, Geology of the Himalayas (L. U. DeSitter, Ed.): New York, John Wiley & Sons, Ltd., 1-308 p.

Graveleau, F., Malavieille, J., and Dominguez, S., 2012, Experimental modelling of orogenic wedges: A review: Tectonophysics, v. 538–540, p. 1–66, doi: 10.1016/j.tecto.2012.01.027.

Guatam, P., and Fujiwara, Y., 2000, Magnetic polarity stratigraphy of Siwalik Groupd seds of Karnali River section in western Nepal: Geophysical Journal International, v. 142, p. 812–824.

Harvey, J.E., Burbank, D.W., and Bookhagen, B., 2015, Along-strike changes in Himalayan thrust geometry: Topographic and tectonic discontinuities in western Nepal: Lithosphere, v. 7, p. 511–518, doi: 10.1130/L444.1.

Hetzel, R., Dunkl, I., Haider, V., Strobl, M., von Eynatten, H., Ding, L., and Frei, D., 2011, Peneplain formation in southern Tibet predates the India-Asia collision and plateau uplift: Geology, v. 39, p. 983–986, doi: 10.1130/G32069.1.

Hodges, K. V., Hurtado, J.M., and Whipple, K.X., 2001, Southward extrusion of Tibetan crust and its effect on Himalayan tectonics: Tectonics, v. 20, p. 799–809, doi: 10.1029/2001TC001281.

Jordan, T.E., Flemings, P.B., and Beer, J.A., 1988, Dating Thrust-Fault Activity by Use of Foreland-Basin Strata, *in* New Perspectives in Basin Analysis, New York, Springer New York, p. 307–330.

Jordan, T.E., 1981, Thrust Loads and Foreland Basin Evolution, Cretaceous, Western United States: AAPG Bulletin, v. 65, p. 2506–2520.

Kirby, E., and Whipple, K.X., 2012, Expression of active tectonics in erosional landscapes: Journal of Structural Geology, v. 44, p. 54–75, doi: 10.1016/j.jsg.2012.07.009.

Kohn, M.J., Wieland, M.S., Parkinson, C.D., and Upreti, B.N., 2004, Miocene faulting at plate tectonic velocity in the Himalaya of central Nepal: Earth and Planetary Science Letters, v. 228, p. 299–310, doi: 10.1016/j.epsl.2004.10.007.

Kohn, M.J., 2008, P-T-t data from central Nepal support critical taper and repudiate large-scale channel flow of the Greater Himalayan Sequence: Geological Society of America Bulletin, v. 120, p. 259–273, doi: 10.1130/B26252.1.

Lallemand, S.E., Schnürle, P., and Malavieille, J., 1994, Coulomb theory applied to accretionary and nonaccretionary wedges: Possible causes for tectonic erosion and/or frontal accretion: Journal of Geophysical Research, v. 99, p. 12033–12055, doi: 10.1029/94JB00124.

Lavé, J., and Avouac, J.P., 2000, Active folding of fluvial terraces across the Siwaliks Hills, Himalayas of central Nepal: Journal of Geophysical Research, v. 105, p. 5735, doi: 10.1029/1999JB900292.

Long, S.P., McQuarrie, N., Tobgay, T., Coutand, I., Cooper, F.J., Reiners, P.W., Wartho, J.A., and Hodges, K. V., 2012, Variable shortening rates in the eastern Himalayan thrust belt, Bhutan: Insights from multiple thermochronologic and geochronologic data sets tied to kinematic reconstructions: Tectonics, v. 31, doi: 10.1029/2012TC003155.

Malavieille, J., 2010, Impact of erosion, sedimentation, and structural heritage on the structure and kinematics of orogenic wedges: Analog models and case studies: GSA Today, v. 20, p. 4–10, doi: 10.1130/GSATG48A.1.

McQuarrie, N., 2002, The kinematic history of the central Andean fold-thrust belt, Bolivia: Implications for building a high plateau: Bulletin of the Geological Society of America, v. 114, p. 950–963, doi: 10.1130/0016-7606(2002)114<0950:TKHOTC>2.0.CO;2.

McQuarrie, N., Tobgay, T., Long, S.P., Reiners, P.W., and Cosca, M.A., 2014, Variable exhumation rates and variable displacement rates: Documenting recent slowing of Himalayan shortening in western Bhutan: Earth and Planetary Science Letters, v. 386, p. 161–174, doi: 10.1016/j.epsl.2013.10.045.

McQuarrie, N., and Ehlers, T.A., 2015, Influence of thrust belt geometry and shortening rate on thermochronometer cooling ages: Insights from thermokinematic and erosion modeling of the Bhutan Himalaya: Tectonics, v. 34, p. 1055–1079, doi: 10.1002/2014TC003783.

McQuarrie, N., and Ehlers, T.A., 2017, Techniques for understanding fold-thrust belt kinematics, and thermal evolution., *in* Linkages and Feedbacks in Orogenic Systems: Geological Society of America Memoir 213, p. 1–30.

Mitra, G., and Boyer, S.E., 1986, Energy balance and deformation mechanisms of duplexes: Journal of Structural Geology, v. 8, p. 291–304.

Molinaro, M., Leturmy, P., Guezou, J.C., Frizon de Lamotte, D., and Eshraghi, S.A., 2005, The structure and kinematics of the southeastern Zagros fold-thrust belt, Iran: From thin-skinned to thick-skinned tectonics: Tectonics, v. 24, p. 1–19, doi: 10.1029/2004TC001633.

Morley, C.K., 1988, Out of Sequence Thrusts: Tectonics, v. 7, p. 539–561, doi: 10.1029/TC007i003p00539.

Mugnier, J.-L., Huyghe, P., Chalaron, E., and Mascle, G., 1994, Recent movements along the Main Boundary Thrust of the Himalayas: Normal faulting in an over-critical thrust wedge? Tectonophysics, v. 238, p. 199–215, doi: 10.1016/0040-1951(94)90056-6.

Mugnier, J.-L., Delcaillau, B., Huyghe, P., and Leturmy, P., 1998, The break-back thrust splay of the Main Dun Thrust (Himalayas of western Nepal): evidence of an intermediate displacement scale between earthquake slip and finite geometry of thrust systems: Journal of Structural Geology, v. 20, p. 857–864, doi: 10.1016/S0191-8141(98)00024-8.

Mugnier, J.-L., Leturmy, P., Mascle, G., Huyghe, P., Chalaron, E., Vidal, G., Husson, L., and Delcaillau, B., 1999, The Siwaliks of western Nepal I. Geometry and kinematics: Journal of Asian Earth Sciences, v. 17, p. 629–642, doi: 10.1016/S1367-9120(99)00038-3.

Mukherjee, S., 2015, A review on out-of-sequence deformation in the Himalaya: Tectonics of the Himalaya, v. 412, p. SP412-SP413, doi: 10.1144/SP412.13.

Murphy, M.A., and Yin, A., 2003, Structural evolution and sequence of thrusting in the Tethyan fold-thrust belt and Indus-Yalu suture zone, southwest Tibet: GSA Bulletin, v. 115, p. 21–34, doi: 10.1130/0016-7606(2003)115<0021:SEASOT>2.0.CO;2.

Najman, Y., Carter, A., Oliver, G., and Garzanti, E., 2005, Provenance of Eocene foreland basin sediments, Nepal: Constraints to the timing and diachroneity of early Himalayan orogenesis: Geology, v. 33, p. 309–312, doi: 10.1130/G21161.1.

Ojha, T.P., Butler, R.F., Decelles, P.G., and Quade, J., 2009, Magnetic polarity stratigraphy of the Neogene foreland basin deposits of Nepal: Basin Research, v. 21, p. 61–90, doi: 10.1111/j.1365-2117.2008.00374.x.

Ojha, T.P., Butler, R.F., Quade, J., DeCelles, P.G., Richards, D., and Upreti, B.N., 2000, Magnetic polarity stratigraphy of the Neogene Siwalik Group at Khutia Khola, far western

Nepal: GSA Bulletin, v. 112, p. 424–434, doi: 10.1130/0016-7606(2000)112<424:MPSOTN>2.0.CO;2.

van der Pluijm, B. a, Hall, C.M., Vrolijk, P.J., Pevear, D.R., and Covey, M.C., 2001, The dating of shallow faults in the Earth's crust.: Nature, v. 412, p. 172–175, doi: 10.1038/35084053.

Rahl, J.M., Haines, S.H., and van der Pluijm, B.A., 2011, Links between orogenic wedge deformation and erosional exhumation: Evidence from illite age analysis of fault rock and detrital thermochronology of syn-tectonic conglomerates in the Spanish Pyrenees: Earth and Planetary Science Letters, v. 307, p. 180–190, doi: 10.1016/j.epsl.2011.04.036.

Ratschbacher, L., Frisch, W., Liu, G., and Chen, C., 1994, Distributed deformation in southern and western Tibet during and after the India-Asia collision: Journal of Geophysical Research, v. 99, p. 19917–19945, doi: 10.1029/94JB00932.

Robinson, D.M., 2008, Forward modeling the kinematic sequence of the central Himalayan thrust belt, western Nepal: Geosphere, v. 4, p. 785, doi: 10.1130/GES00163.1.

Robinson, D.M., DeCelles, P.G., and Copeland, P., 2006, Tectonic evolution of the Himalayan thrust belt in western Nepal: Implications for channel flow models: GSA Bulletin, v. 118, p. 865–885, doi: 10.1130/B25911.1.

Robinson, D.M., DeCelles, P.G., Patchett, P.J., and Garzione, C.N., 2001, The kinematic evolution of the Nepalese Himalaya interpreted from Nd isotopes: Earth and Planetary Science Letters, v. 192, p. 507–521, doi: 10.1016/S0012-821X(01)00451-4.

Robinson, D.M., and Martin, A.J., 2014, Reconstructing the greater indian margin: A balanced cross section in central Nepal focusing on the lesser himalayan duplex: Tectonics, v. 33, p. 2143–2168, doi: 10.1002/2014TC003564.

Robinson, D.M., and McQuarrie, N., 2012, Pulsed deformation and variable slip rates within the central Himalayan thrust belt: Lithosphere, v. 4, p. 449–464, doi: 10.1130/L204.1.

Rohrmann, A., Kapp, P., Carrapa, B., Reiners, P.W., Guynn, J., Ding, L., and Heizler, M., 2012, Thermochronologic evidence for plateau formation in central Tibet: By 45 Ma: Geology, v. 40, p. 187–190, doi: 10.1130/G32530.1.

Sakai, H., 1983, Geology of the Tansen group of the Lesser Himalaya in Nepal: Memoirs of the Faculty of Science, Kyushu University. Series D, Geology, v. 25, p. 27–74.

Shaw, J.H., Bilotti, F., and Brennan, P.A., 1999, Patterns of imbricate thrusting: Bulletin of the Geological Society of America, v. 111, p. 1140–1154, doi: 10.1130/0016-7606(1999)111<1140:POIT>2.3.CO;2.

Suppe, J., 1980, Imbricate structure of western foothills belts, south-central Taiwan: Petroleum Geology of Taiwan, v. 17, p. 1–16.

Szulc, A.G., Najman, Y., Sinclair, H.D., Pringle, M.S., Bickle, M., Chapman, H., Garzanti, E.,

Andó, S., Huyghe, P., Mugnier, J.-L., Ojha, T.P., and DeCelles, P.G., 2006, Tectonic evolution of the Himalaya constrained by detrital 40Ar-39Ar, Sm-Nd and petrographic data from the Siwalik foreland basin succession, SW Nepal: Basin Research, v. 18, p. 375–391, doi: 10.1111/j.1365-2117.2006.00307.x.

Tobgay, T., McQuarrie, N., Long, S., Kohn, M.J., and Corrie, S.L., 2012, The age and rate of displacement along the Main Central Thrust in the western Bhutan Himalaya: Earth and Planetary Science Letters, v. 319–320, p. 146–158, doi: 10.1016/j.epsl.2011.12.005.

Turcotte, D.L., and Schubert, G., 1982, Geodynamics: New York, John Wiley, 450 p.

Vrolijk, P., and Van Der Pluijm, B.A., 1999, Clay gouge: Journal of Structural Geology, v. 21, p. 1039–1048, doi: 10.1016/S0191-8141(99)00103-0.

Xie, X., and Heller, P.L., 2009, Plate tectonics and basin subsidence history: Bulletin of the Geological Society of America, v. 121, p. 55–64, doi: 10.1130/B26398.1.